Studies on the Recombinant Mutants of the Cys-298 Residue of Human Aldose Reductase

by

Emeka J. Udeigwe

Submitted in Partial Fulfillment of the Requirements

for the Degree of

Master of Science

in the

Chemistry

Program

YOUNGSTOWN STATE UNIVERSITY

August, 2015

Studies on the Recombinant Mutants of the Cys-298 Residue of Human Aldose Reductase

Emeka J. Udeigwe

I hereby release this thesis to the public. I understand that this thesis will be made available from the OhioLINK ETD Center and the Maag Library Circulation Desk for public access. I also authorize the University or other individuals to make copies of this thesis as needed for scholarly research.

Signature:

_____

Emeka J. Udeigwe, Student Date

Approvals:

_____

Dr. Ganesaratnam K. Balendiran, Thesis Advisor Date

_____

Dr. Sherri Lovelace-Cameron, Committee Member Date

_____

Dr. Brian D. Leskiw, Committee Member Date

_____

Dr. Salvatore A. Sanders, Associate Dean of Graduate Studies Date

THESIS ABSTRACT

The enzyme human aldose reductase (hAR*)* catalyzes the NADPH-dependent reduction of glucose to sorbitol. hAR is part of the polyol pathway and it exists in the native and the activated form. Of the three cysteine residues in hAR, located on the active site, the Cys-298 residue is prone to oxidative modification. Previous studies have reported that the Cys-298-Ser mutant shows similar characteristics as the activated enzyme, and include an increased V_{max} and K_m, a comparatively low k_{cat}/K_m and a large K_i value. Using site-directed mutagenesis of Cys-298 to Asparagine and Glutamate (Cys-298-Asn and Cys-298-Glu respectively), and DL-Glyceraldehyde as the substrate, the Cys-298-Asn mutant displayed a 60% increase in K_m, a 65% decrease in k_{cat} and an 18% increase in k_{cat}/K_m. The Cys-298-Glu mutant, however, displayed an increased K_m, >3-fold, a 49% decrease in k_{cat}, and a decreased k_{cat}/k_m (up to 84%). The increased K_m the Cys-298-Glu mutant enzyme demonstrates a reduced affinity for the substrate compared to the wild-type, suggesting a likelihood that the interaction of NADPH with the enzyme is weakened, hence a reduced conformational change of the enzyme-NADPH binary complex and a weaker substrate binding. It is possible that glutamic acid, an acidic, polar amino acid destabilizes the NADPH and the substrate-binding site. The increased K_m and k_{cat} of the Cys-298-Asn mutant shows an expected trend, due to the hydrophobic nature of asparagine and the ability of its carboxyamide group to form a hydrogen bond with neighboring residues on the active site pocket. The hydrogen bonding would permit the tight binding of NADPH to the enzyme, and the increased formation of the enzyme-NADPH binary complex. These results present facts about these mutants that have not been previously studied.

ACKNOWLEDGEMENT

My sincere gratitude goes to my advisor, Dr. Ganesaratnam Balendiran for the incredible opportunity to work in his research group, his support and guidance throughout the duration of this project and my studies, his consistent advice and his resilient spirit to ensure that I surpass my limitations. To Sudipti Gupta, for her enthusiastic and dauntless role in this research and for the indelible part she played in this project. My deepest appreciation also goes to the head, faculty and staff of the Chemistry Department for their support in ensuring the completion of my program. I would like to thank Dr. Sherri Lovelace-Cameron and Dr. Brian Leskiw for the privilege of being my committee members, especially to Dr. Sherri Lovelace-Cameron for her endless willingness to address my numerous concerns. To the members of my lab: Dan, DaVena, Heather, Amanda, Niloufar, Brian, Tamer and Nate. Working with this group of students has been nothing short of inspiring. To my good friend, Charles, for his encouragement when the going was tough; I could never ask for a better human being. I also need to thank most desperately my family, who has been the greatest support I have had my entire life. My brothers, Dr. Lawrence and Dr. Theo, for believing in me and giving me the support that I needed to become who I am today. To my mother, thank you for all your love and prayers, and to all my siblings for their constant support. Not to forget that this study would not have been possible without the immense contribution of Grant, DK085496, from the National Institutes of Health and the American Diabetes Association.

TABLE OF CONTENTS

LIST OF TABLES

LIST OF FIGURES

LIST OF SYMBOLS AND ABBREVIATIONS

%	Percent
©	Copyright
®	Registered
Abs	UV-Vis absorbance
AGEs	Advanced glycation end-products
AKR1A1	Aldehyde reductase
AKR1B1	Aldose reductase
AKRs	Aldo-keto reductase
ALR2: WT	Wild-type aldose reductase
Amp	Ampicillin
BME	β-mercaptoethanol
Bp	Base pair
C	Cytidine
C298S	Cysteine to serine mutation at the 298th position
C303S	Cysteine to serine mutation at the 303rd position
C80S	Cysteine to serine mutation at the 80th position
$CaCl_2$	Calcium chloride
Cys	Cysteine
Cys-298-Asn	Cysteine to asparagine mutation at the 298th position
Cys-298-Glu	Cysteine to glutamic acid mutation at the 298th position
Cys-298-Ser	Cysteine to serine mutation at the 298th position
ddH_2O	Double deionized water
DNA	Deoxyribonucleic acid
dNTP	Dinucleotide triphosphate
Dpn	Diplococcus pneumonia G41

dsDNA	Double stranded DNA
DNTB	5,5'-dithiobis(2-nitrobenzoic acid)
DTT	Dithiothrietol
G	Guanine
Glu	Glutamic acid
GS-DHN	Glutathionyl-1,4-dihydroxynonene
GSH	Glutathione
GSH-HNE	Glutathionyl-4-hydroxynonenal
GSNO	S-nitrosoglutathione
GSSG	Glutathione disulfide
hAR	4-hydroperoxy-2(E)-nonenal
HEPES	4-(2-hydroxyethyl)-1-piperazineethanesulfonic acid
HHE	4-hydroxy-2(E)-hexenal
His	Histidine
IMAC	Immobilized metal affinity chromatography
IPTG	isopropyl-1-thio-β-D-galactopyranoside
K	Kilo
k_{cat}	Turnover number
k_{cat}/K_m	Catalytic efficiency
KCl	Potassium chloride
KH_2PO_4	Potassium phosphate
K_i	Inhibition constant
K_m	Michaelis-menten constant
LB	Luria-broth
Lys-77	Lysine residue at the 77^{th} position of aldose reductase
M	Molar
$m^{-1}cm^{-1}$	Per molar per centimeters

MES	4-morpholineethanesulfonic acid
mg	Milligram
mg/mL	Milligram per milliliter
mL	Milliliter
mM	Millimolar
MWCO	Molecular weight cut off
NaCl	Sodium chloride
NAD^+	Oxidized form nicotinamide adenine dinucleotide
NADH	Reduced form nicotinamide adenine dinucleotide
$NADP^+$	Oxidized form of nicotinamide adenine dinucleotide phosphate
NADPH	Reduced form of Nicotinamide adenine dinucleotide phosphate
NF- κB	Nuclear factor kappa-light-chain-enhancer of activated B-cells
ng	Nanogram
nm	Nanomoles
nmol/min	Nanomoles per minutes
nmol/s	Nanomoles per seconds
$O.D_{595}$	Optical density at 595 nanometers
PAGE	Poly-acrylamide gel electrophoresis
PBS	Phosphate buffered saline
PCR	Polymerase chain reaction
PK(C)	Protein kinase C
pKa	Negative log of Ka
rpm	Revolutions per minutes
S	Seconds
SDS	Sodium-dodecyl sulfate

Ser-298	Serine residue at the 298th position
SOC	Super optimal broth with catabolite repression
T	Thymidine
TEMED	Tetramethylethylenediamine
TIM	Triose-phosphate isomerase
Tm	Melting temperature
TNF-α	Tumor necrosis factor-alpha
Tyr-48	Tyrosine residue at the 48th position
U	Unit
V	Volts
v/v	Volume per volume
V_{max}	Maximum velocity
w/v	Weight per volume
X-Gal	5-bromo-4-chloro-3-indoyl-β-D-galactopyranoside
Y48H	Tyrosine to histidine mutation at the 48th position
Y48S	Tyrosine to serine mutation at the 48th position
Y50F	Tyrosine to phenylalanine mutation at the 50th position
µg	Microgram
µL	Microliter
µM	Micromolar
$\Delta Abs_{340}/\Delta T$	Change in absorbance at 340nm per change in time

1.0 INTRODUCTION

The regulation of intracellular glucose, which cells use for energy is of crucial significance in maintaining homeostasis. Among the mechanisms of this regulation are glycolysis and the pentose phosphate pathway, both utilizing the glucose phosphorylated by hexokinase, which is then fed through the pathway to the final products [5]. Several glycemic regulation of organisms, are significantly contingent on the interactions and or strengthening of these mechanisms, making glycemic control clearly effective in reducing the incidence and progression of diseases that are associated with the malfunction of these systems; such as retinopathy [24], neuropathy and nephropathy. Diseases such as Diabetes Mellitus, for instance, are highly characterized by chronic hyperglycemia, as well as deficit in insulin secretion, action or both. These circumstances greatly lead to the obliteration of the natural pathways in which the levels of glucose are balanced [2]. Furthermore, chronic elevation of glucose alters the biochemical homeostasis of cardiovascular cells by impacting a number of vital biochemical pathways, including the cytoplasmic redox state, the protein kinase (PK) C pathway, and the glucosamine biosynthesis pathway, leading to the production of intracellular glycating species [69], [44], [13], [37], [33]. This knowledge, taken together, has spurred contentions if other pathways are upregulated in response to the expenditure of systems involved in glucose regulation, and if these pathways explain secondary diabetic complications implicated in diabetic tissues.

Several pathways have been linked to be compensatory to elevated glucose levels. One of such pathway is the Polyol pathway [24], which accounts for about 33% of the

glucose flux in some tissues in hyperglycemic conditions [16]. Indications of the polyol pathway as a contributor to diabetic complications such as retinopathy have been examined in the galactosemic models [21], [20], [55], diabetic rats [54] and in diabetic dogs and galactose-fed dogs [19]. Interestingly, the concept of the polyol pathway and how it relates to diabetic neuropathy have also been studied [24].

1.1 OVERVIEW OF RELATED TOPICS

1.1.1 The Polyol Pathway

The polyol pathway (Figure 1.1) of glucose metabolism is a two-step metabolic pathway in which glucose is reduced to sorbitol. This pathway primarily becomes activated when the intracellular levels of glucose are elevated [23], [44], such as in diabetes mellitus and galactosemia. Collectively, two enzymes are involved in this pathway – aldose reductase and sorbitol dehydrogenase; each of which are present in human tissues and organs that are the site of diabetic complications, such as eye (retinal ganglion cells, lens), kidney and the myelin sheath [59]. The product of the polyol pathway and the imbalance of cofactors generate the types of cellular stress that occur at the site of diabetic complications [42].

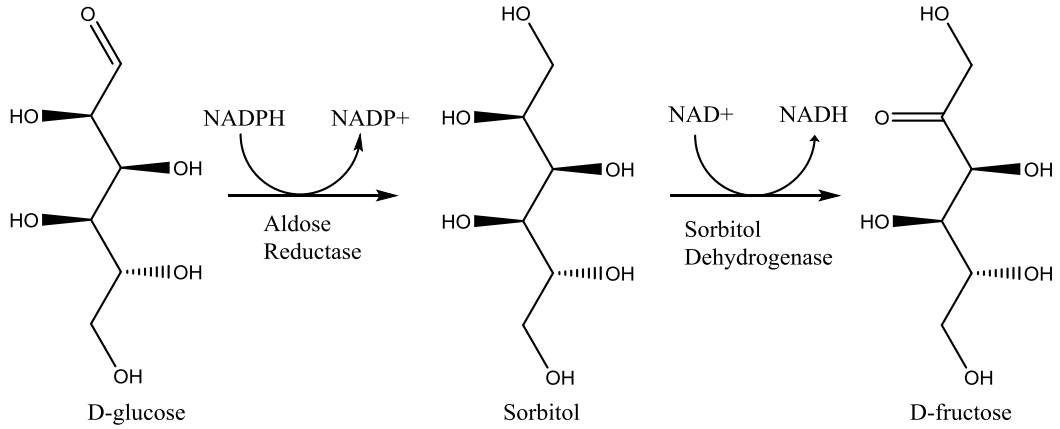

Figure 1.1: The polyol pathway. Two-step enzymatic reaction where D-Glucose is reduced to sorbitol by aldose reductase, with the generation of $NADP^+$. Sorbitol is oxidized to fructose by sorbitol dehydrogenase, with the production of NAD^+.

As shown in Figure 1.1, Aldose reductase, the first enzyme in the pathway is the rate-limiting step of the pathway and catalyzes the reduction of glucose to sorbitol, using NADPH as a cofactor, which is oxidized to $NADP^+$. Sorbitol (glucitol) is then oxidized to fructose by sorbitol dehydrogenase, which uses NAD^+ as a cofactor, with the associated generation of NADH. The progression of the polyol pathway continuously generates the metabolite sorbitol, a strongly hydrophilic alcohol, which is impermeable to cell membranes and accumulates intracellularly, becoming trapped in cells, like the retinal cells and Schwann cells. This buildup generates osmotic imbalance, triggering retinopathy, cataracts and peripheral neuropathy [24], [44]. Fructose-3-phosphate and 3-deoxyglucosone, which are both potent glycosylating agents, can be generated from this pathway. The former is produced by the phosphorylation of fructose, while the latter is generated by the hydrolysis of fructose-3-phosphate and has been identified in the lens of diabetic rats [65].

Research has shown that several mechanisms of cellular damage can occur following the recruitment of the polyol pathway. These damages, aside from the possible formation of advanced glycation end products (AGEs) by fructose-3-phosphate and the 3-deoxyglucosone, may result from the depletion of NADPH. The resultant effect could cause altered intracellular tonicity, decreased synthesis of reduced glutathione (GSH), increased activity of the glucose monophosphate shunt [2], and pseudohypoxia [71]. Generally, the activation of the polyol pathway leads to the exposure of cells to oxidative stress, through the reduced action of antioxidants such as GSH, all of which are implicated in the development of diabetic complications.

1.1.2: Aldo-keto reductases.

Aldo-keto reductases comprise a superfamily and a collection of diverse proteins with several functions, such as biosynthesis, intermediary metabolism and detoxification. Substrates of aldo-keto reductases include glucose, steroids, glycosylation end – products, environmental pollutants, and lipid peroxidation products such as HNE (4-hydroxynonenal). Aldo-keto reductases are structurally related by a TIM (triose-phosphate isomerase) - barrel structural motif, and they mostly catalyze oxidation-reduction reactions. This motif represents a structure required for the binding of a diverse range of carbonyl substrates, such as glucose [25], using nucleotides such as NADPH, as cofactor for the aldehyde reduction reactions, and oxidized nucleotides like NAD^+ as the cofactor for the reverse reaction. All plants and animals ranging from yeast to man are thought to express multiple *Akr* (Aldo-keto reductase) genes. However it is difficult to draw a line between aldo-keto reductase from lower organisms and those of higher

organisms because the aldo-keto reductases from lower organisms form their own sub-families.

Aldo-keto reductases as oxidoreductases have a distinguishing feature regarding their ability to catalyze the reduction of both aldehydes and ketones. Most aldo-keto reductases prefer NADPH to NADH; $NADP^+$ is mostly in the reduced form in metabolically active cells, which favors reduction. The $NADPH/NADP^+$ ratio is reflective of the synthetic capacity of the cell and is kinetically different from the $NAD^+/NADH$ ratio, which is mostly regulated by the rates of respiration and glycolysis. Aldo-keto reductases therefore accomplishes metabolism without being affected by fluctuations in the cofactor ratio due to changes in the rate of metabolism.

1.1.3: Basic Structural Features of Some Aldo-Keto Reductases

Aldo-keto reductases are widely distributed in tissues, and about 13 different aldo-keto reductase proteins have been identified in humans that fall within 3 major families of mammalian aldo-keto reductases. Aldo-keto reductases share a $(\beta/\alpha)_8$ barrel structure with either a $NADP^+$ or a NADPH binding site. The aldo-keto reductase superfamily is divided into 15 families, with some subfamilies. There exists about 40% homology of these proteins with each other.

The $(\beta/\alpha)_8$ motif of aldo-keto reductases is believed to result from fusion of half barrel protein and gene duplication [32] with different functionalities such as binding redox active cofactors and metals [68], or used as a gated barrel for channeling reaction intermediates [4]. The $(\beta/\alpha)_8$ barrel fold is distinguished by the presence of the active site at the C-terminus, considered to be indicative of a common ancestry from progenitor

proteins of broader substrate specificity. Another conserved feature of $(\beta/\alpha)_8$ proteins is the presence of a phosphate binding site. Approximately two-thirds of the established $(\beta/\alpha)_8$ barrel enzymes utilize substrates or cofactors that contain a phosphate group. In the aldo-keto reductase family this is the pyrophosphate backbone of the pyridine nucleotide.

1.1.4 Aldose Reductase

Aldose reductase is a cytosolic NADPH-dependent oxidoreductase, which belongs to the superfamily of the aldo-keto reductases – enzymes that catalyze aldehyde or ketone reduction to their corresponding alcohols, utilizing purine nucleotides. Aldose reductase was first identified as a protein with glucose reducing activity in 1960 [31], but has since then been extensively studied and characterized due to its potential role in mediating hyperglycemic injury and in the development of secondary diabetic complication [24]. In the polyol pathway, the reaction catalyzed by aldose reductase represents the rate-limiting step of the pathway.

Inhibitors of aldose reductase have been shown to delay or inhibit tissue injuries linked to diabetic complications [22], [12] in animal models. However, the amelioration of these tissue injuries has not been completely established in diabetic patients, due of limited efficacy. Ramana *et al*., (2007) [53], indicated in their studies that the specific mechanism in which aldose reductase aids in the tissue injury is related to the enzyme's ability to mediate several inflammatory pathways, such as high glucose-induced vascular smooth muscle cell growth, through high glucose triggered release of tissue necrosis factor-alpha (TNF-α), a major proinflammatory cytokine. For instance, aldose reductase

plays a role in mediating mitogenic signaling triggered by cytokines [50], and aids proliferation of smooth muscles during atherosclerosis. Hence, inhibition of aldose reductase attenuates TNF-α, growth factor-induced activation of NF-κB and apoptosis of human lens epithelial cells [51]. Nonetheless, the mechanism by which this regulation occurs remains uncertain.

Aldose reductase has broad reduction specificity to several substrates like lipid peroxidation products such as HNE, AGE precursors [37], isocorticosteroids [70], and glutathione conjugates of unsaturated aldehydes such as GS-HNE [62]. Aldose reductase is also known as the low K_m aldehyde, in contrast to other families of the aldo-keto reductases with higher catalytic efficiency (k_{cat}/K_m) for most substrates but a lower k_{cat} [10]. In the catalysis of the enzyme, as would be explained further in this chapter, nucleotide exchange is the rate-limiting step, hence the turnover number (k_{cat}) is substrate-independent [9].

1.1.5 Variations, Topology and Structural Features of Aldose Reductases.

The amino acid sequence of aldose reductase is represented in Figure 1.2. In this figure, the $(\beta/\alpha)_8$ motif is formed by a hairpin of two β-strands (β1 and β2), which forms the bottom of the barrel [45]. The $(\beta/\alpha)_8$ barrel itself is surrounded by several loops and helixes that differ between several aldo-keto reductases and that confer individuality to different aldo-keto reductase families [45]. The "hot spot" for such variations is the region between the 7th and the 8th β-strands of the barrel (strands β9 and β10 in aldose reductase, Figure 1.2) [45].

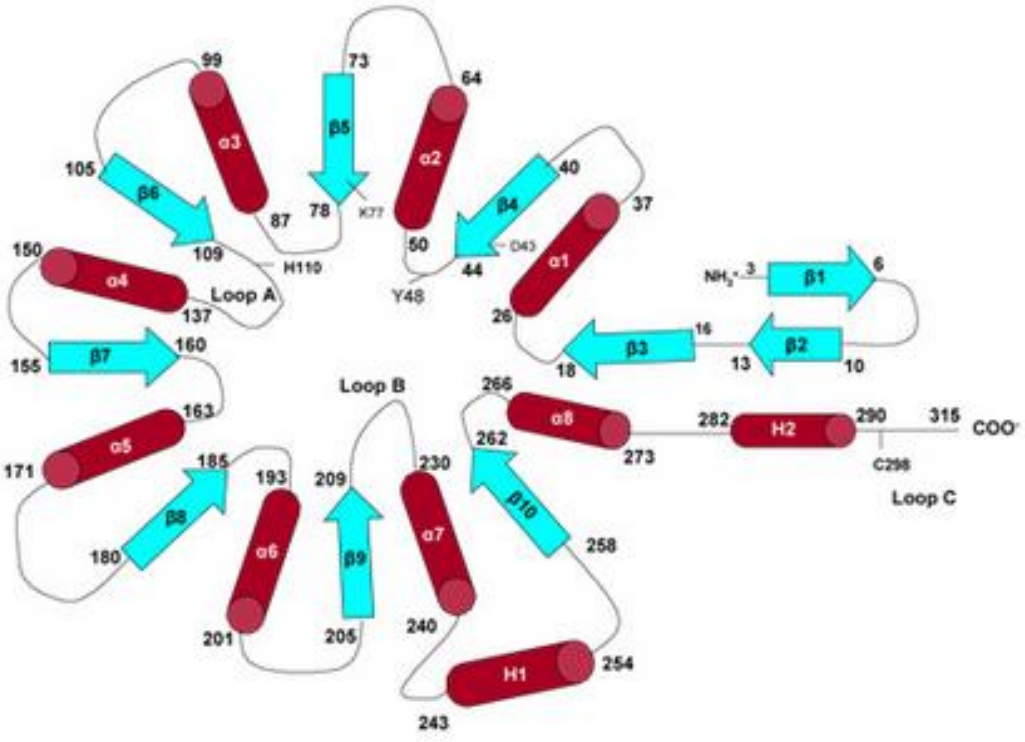

Figure 1.2: Topical representations of amino-acid sequence of aldose reductase. The β strands (blue) are represented as arrows and the α-helices (red) as cylinders. Each major strand and loop is numbered. Connecting random coils are shown as extended loops. The position of the active-site residue in sequence is indicated [45].

The sequence and structure of these extraneous elements differ between subfamilies and is a distinctive feature for a particular subfamily of the enzyme. For example, aldehyde and aldose reductases have a long loop between β9 and α7 (residues 209 to 230 in aldose reductase) - loop B, Fig. 1.2, that opens and closes as soon as a nucleotide comes in to bind [73], thus accelerating tight binding to NADPH. The length of this loop is variable among members of the family and in some aldo-keto reductases, for example, the characteristic small size of hydroxysteroid dehydrogenases [4], results in

the absence of the opening or closing movement of the loop B that is found in its structure.

1.1.6 Catalytic Mechanism of Aldose Reductase

Different families of the aldo-keto reductases are effective in catalyzing some reactions better than the others. The aldehyde and the aldose reductases are more efficient in catalyzing reduction, whereas other aldo-keto reductases e.g., hydroxysteroid dehydrogenases and dihydrodiol reductases are equally effective as reductases or dehydrogenases [46].

Structurally, most aldo-keto reductases are composed of a catalytic tetrad with different functionalities, consisting of Tyr-48, His-110, Lys-77 and Asp-43, with the pK_a ranging from 6.5 to 7.0 [17]. Based on the low pK_a, Tyr-48, unlike His-110, is conserved in most aldo-keto reductases [45]. Acid-base catalysis is involved in the oxidation reaction of aldose reductase. Studies using human aldose reductase complexed with NADPH show three residues that could hypothetically function as the proton donor in the catalytic mechanism: Tyr-48, His-110, and Cys-298 [73], [29]. Kinetic studies and structural modeling provided compelling evidence that Tyr-48 is the most likely proton donor [27], [28] in aldose reductase catalysis, functioning as an acid catalyst with its hydroxyl group within hydrogen bonding distance of the underlying ammonium side chain of Lys-77. His-110 was first suggested to be the acid-base catalytic group for aldose reductase [17] but however, later studies by Bohren *et al*., (1994), using a mutant Y48F, showed that it was inactive, whereas mutations of His-110 resulted in the generation of a partially active enzyme, suggesting that the acid-base catalytic group in aldo-keto reductases is Tyr-48. His-110 was however subsequently proposed to play an

important role in proper orientation of the substrate at the active site. The studies on the role of Tyr-48 and His-110 was corroborated by crystallographic studies, which showed that zopolrestat, an aldose reductase inhibitor, binds with high affinity at the active site of the enzyme [72]. Zopolrestat contains a carboxylate functional group, and carries a carboxylate oxygen atom, which is within a distance of 2.65Å to the phenolic hydroxyl of Tyr-48. The carboxylate oxygen atom would be similar to the carbonyl oxygen of aldehyde substrates that aldose reductase reduces. Likewise, the carbonyl carbon of zopolrestat, similar to an aldehyde substrate carbonyl carbon, was separated at 3.63Å from the nicotinamide C-4 of NADPH.

As shown in Figure 1.3, aldose reductase reduction proceeds via a concerted or step-wise two-step mechanism: 1) Transfer of a hydride ion from NADPH to the carbonyl substrate, and 2) addition of a proton from the solvent to reduce the carbonyl to its corresponding alcohol. In complex I, (Figure 1.3), Tyr-48 on the active site, forms a hydrogen bond with the substrate carbonyl group [45], resulting in the carbonyl polarization shown above and the acceleration of the hydride transfer of the pro-R hydrogen from the nicotinamide ring of NADPH to the carbonyl carbon of the substrate [45]. Proton transfer is made easier by the hydrogen-bonding interaction of Lys-77 and Asp-43, which lowers the pK_a of tyrosine [9]. Several observations, however, do not support an obligatory role of tyrosine in catalysis of aldose reductase. For instance, Y48H and Y48S mutants of aldose reductase retain catalytic activity [9], but Y50F mutation in aldehyde reductase does not bind to carbonyl substrates and does not proceed with the catalytic mechanism of the enzyme, implying that the tyrosine at the active site is crucial in substrate binding. Complex II (Figure 1.3) results from a transition state in which the

polarization at the carbonyl is reduced by the proton transferred from Tyr-48 and a concerted hydride transfer to the carbonyl carbon [45]. In complex III (Figure 1.3), the reduced carbonyl dissociates from the acid-base catalyst resulting in a net charge on the tyrosinate anion, which is stabilized by the hydrogen-bonding network [45].

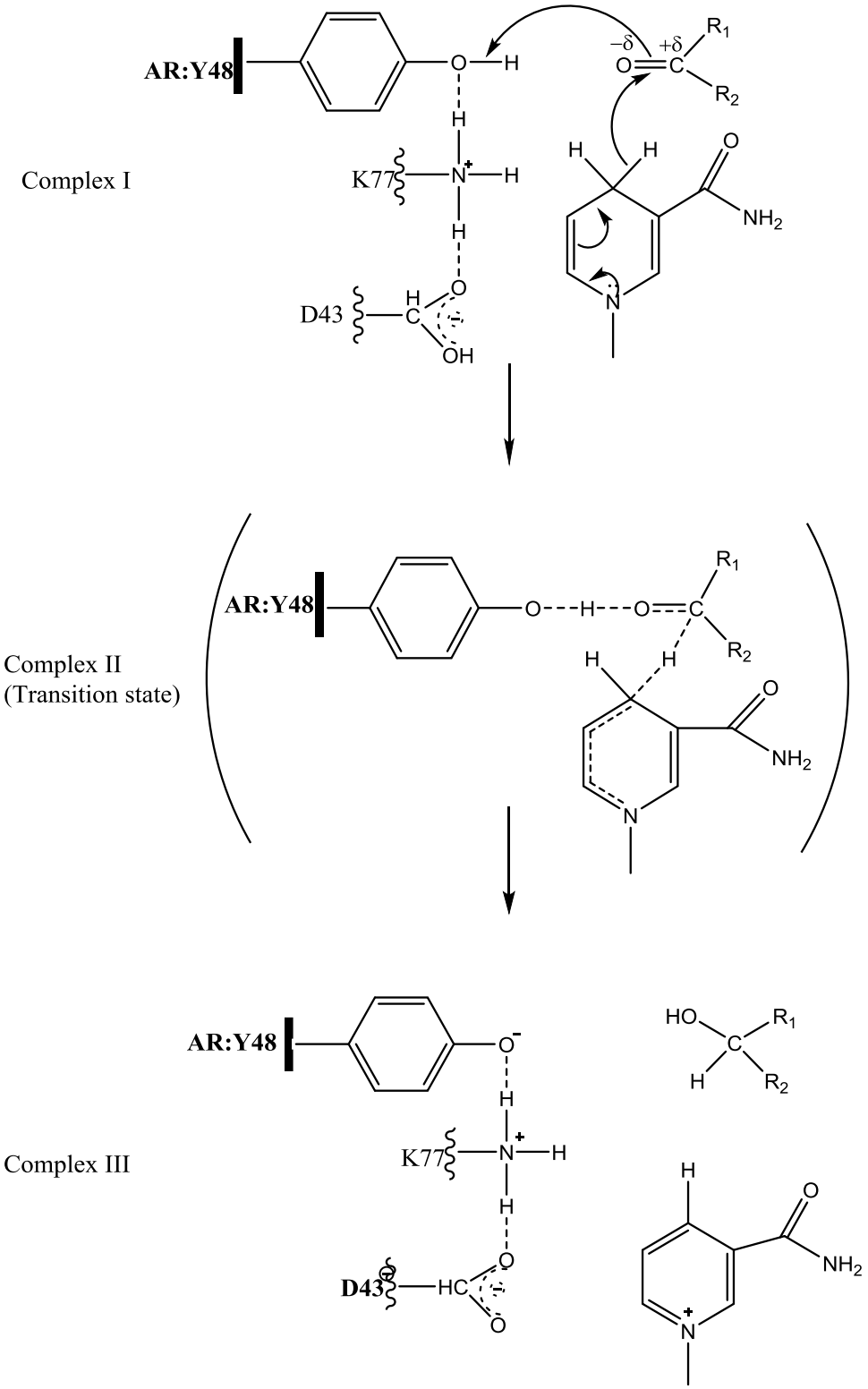

Figure 1.3: Catalytic mechanism of common aldo-keto reductases - aldose reductase [45].

Mechanistically, aldose reductase proceeds via a sequential ordered (Bi-Bi) mechanism in which the cofactor NADPH binds first to the enzyme. The binding of NADPH to the enzyme results in a conformational change (E•NADPH →*E•NADPH), involving a hinge-like movement of a surface loop, involving residue 213-217 so as to cover a portion of the NADPH [43]. The substrate further binds to the binary complex that is formed, and the alcohol product is formed by the transfer of a pro-R hydride of NADPH to the re-face of the substrate's carbonyl carbon. The hydride that is transferred from NADPH to an aldehyde comes from the C-4 of the nicotinamide ring. Another conformational change (*E•$NADP^+$→E•$NADP^+$) occurs, following the release of the alcohol product, which then leads to the release of $NADP^+$ [43], [38]. This kinetically significant structural isomerization is thought to represent the rate-limiting step in the direction of aldehyde reduction [38], [27], making *E•$NADP^+$ the predominant enzyme form at steady state. Tight binding of NADPH to aldose reductase leads to a thermodynamic advantage for achieving the transition state without placing much constraint on the substrate. As most of the energy required for carbonyl reduction is derived from nucleotide (NADPH), even substrates that are loosely bound to active site residues are reduced with high efficiency. As a result, aldose reductase is capable of reducing a wide range of aldehydes.

Aldose reductase is said to be very sensitive to oxidation. Oxidation of one of its cysteine residues (Cys-298), located at the active site accelerates catalysis and prevents inhibitor binding [47]. Accelerated catalysis and enzyme activity has been linked to a decrease in the affinity of the enzyme for NADPH [18]. Oxidation of Cys-298 prevents complete closure of the NADPH binding loop and therefore the loop is easier to open

during the release of $NADP^+$ [6]. Because $NADP^+$ release is the rate-limiting step in aldose reductase catalysis [27], an increase in the rate of $NADP^+$ release increases k_{cat}. Several experimental studies indicate that oxidation of Cys-298 is a physiological process and that it symbolizes a form of redox regulation. Hence Cys-298 of aldose reductase could be nitrosylated, glutathiolated, or oxidized to a sulfenic acid, sulfinic acid, and sulfonic acid. Other studies have also been able to show that glutathiolated and sulfenic acid forms of aldose reductase have been identified *in vivo* [35], [60], [64], [49].

X-ray structure determination have been able to explain that the active site of aldose reductase lacks ionic residues that are characteristics of polyol-binding proteins but mostly have hydrophobic residues at this site. This characteristic makes hydrophobic aldehyde as the preferred substrate for aldose reductase [11]. Furthermore, isolated aldose reductase has very low affinity for some aldehydes, and the hydrophobicity of the substrate-binding domain in the active site of the enzyme inhibits efficient carbohydrate reduction, such as glucose. This is explained by the high K_m exhibited by the reaction of glucose with aldose reductase [11].

1.1.7 Native and Activated Forms of Human Aldose Reductase.

Human aldose reductase (hAR) exists in both a native and an activated form (inhibitor-resistant form). The activated form of hAR poses a challenge to the development of diabetic drugs. The extent of the activation of hAR is the key to the unresponsiveness of any diabetic to a given aldose reductase inhibitor therapy. Experimental kinetic studies of hAR have been able to establish differences in kinetic parameters between activated and native hAR. These differences are shown by increases

in K_m and V_{max} for aldehyde substrates and increases in k_i. Liu *et al*; (1992), demonstrated that carboxymethylation of aldose reductase results to an enzyme form with different altered susceptibility to inhibitors like Tolrestat and sorbinil [40], resulting in the conclusion that different inhibitor binding site exists on aldose reductase. In addition, activated aldose reductase displaying reduced sensitivity to different aldose reductase inhibitors have been understood to be generated through isomerization, glycosylation [61], and thiol-dependent oxidation [40]. Grimshaw *et al*., (1996), reported the purification of human aldose reductase, and proved that about 20% of the aldose reductase activity freshly purified from human placenta exhibit kinetic properties and inhibitor insensitivity consistent with those described for the activated or oxidized enzyme form, using a sensitive Sorbinil titration assay. Hence, the level of insensitivity to aldose reductase inhibitor therapy and the susceptibility to secondary diabetic complications is judged by the extent of activation of human aldose reductase *in vivo*.

Detection of the activated form of human aldose reductase has been a controversial topic. Vander Jagt *et al*., (1990), demonstrated that dialysis in the presence of high salt concentration, which occurs in purification following ammonium sulfate precipitation can lead to the formation of the activated enzyme form. Vander Jagt *et al*., 1990, further showed that when aldose reductase was purified in the presence of $NADP^+$ and without any thiol reducing agents, there was little or no formation of the activated enzyme form during the purification process, since the $NADP^+$ protects and stabilizes the enzyme against post-translational modification. However, as this activation occurs to form the oxidized enzyme, the general consensus is that the activated enzyme form is less susceptible to inhibition by most aldose reductase inhibitors.

1.2: RELATED WORK

Much effort has been invested in understanding the nature of the activated human aldose reductase, by addressing the kinetic parameters of activated and native hAR. These efforts have been instrumental in understanding the key residues involved in the catalysis of aldose reductase using molecular biology techniques such as site-directed mutagenesis**.** Grimshaw *et al*., (1996), in his research demonstrated the significant kinetic differences between the recombinant native and oxidized enzyme forms and the human placental native and oxidized enzyme forms of aldose reductase.

In Table 1.1, Grimshaw *et al*., (1996), utilized an efficient and a rapid purification method in the purification of the enzyme used in this study, in order to reduce the possibility of a rapid conversion of the enzyme to the activated form. Using DL-Glyceraldehyde as substrate as presented in Table 1.1, the K_m for the oxidized enzyme increases from 0.047mM to 2.4mM and 0.024mM to 6.8mM when compared to the native and oxidized enzyme forms, for the recombinant enzyme and human placental enzyme respectively, while the V_{max} varied slightly (shown as increase). The higher V_{max} for the oxidized form of the human placental aldose reductase, from Table 1.1 explains that the oxidized forms of the enzyme reaches a maximum rate faster than the native form. The increase in the K_m of the oxidized enzyme describes that the amount of substrate needed for the oxidized enzyme to reach half of its maximum rate (velocity) is greater than the native enzyme. The net effect is almost a 50-fold decrease in the catalytic efficiency (k_{cat}/K_m) for the oxidized recombinant enzyme form and about a 120-fold decrease in the k_{cat}/K_m for the aldehyde reduction by the oxidized human placental enzyme form. This decrease in the catalytic efficiency of oxidized hAR, represented as

(V/K), means that it can catalyze the forward reaction less efficiently than the native hAR, as the catalytic efficiency for the native enzyme was greater than that of the oxidized enzyme.

Table 1.1: Kinetic parameters for native and oxidized aldose reductase, determined using either recombinant wild-type hAR or aldose reductase isolated from human placenta [26]. As reported by Grimshaw *et al*., (1996)

Comparison of Kinetic Parameters for Native and Oxidized Aldose Reductase [26]

	Recombinant Enzyme		Human Placenta	
Parameter[a]	Native	Oxidized	Native[b]	Oxidized[c]
V (s^{-1})	0.45	0.50	0.62	1.5
K(mM)	0.047	2.4	0.024	6.8
V/K($mM^{-1}s^{-1}$)	9.6	0.21	26	0.22
$K_{i\ (Sorbinil)}$	0.5	380	0.5	400

[a]DL-glyceraldehyde. Mops buffer (pH 7.0). 25°C.

[b]Average results for low K_m region velocities for several human placenta ALR2 sample.

[c]Results from single 100% oxidized human placenta ALR2 sample.

Clearly, activated hAR has a detrimental effect on inhibitor potency and enzyme-substrate interaction as demonstrated on Table 1.1. In addition, the difference in the kinetic parameters and aldose reductase inhibitor potency between the native and oxidized enzyme form is similar for either enzyme source (recombinant and human placental tissues). There also appears to be nearly 1000-fold loss in aldose reductase inhibitor potency using an otherwise potent inhibitor, sorbinil. The higher K_i for the activated hAR, shown in Table 1.1, reveals that a higher concentration of sorbinil was required to decrease the V_{max} by one half. Activated human aldose reductase hence has a negative effect on the potency of inhibitors, such as sorbinil.

The activated human aldose reductase detected in fresh placenta by the researchers, was also suggested to be due to the mixed disulfide with thiol containing compounds such as glutathione [14]. This mixed disulfide could result from the cyteine residues of the protein becoming oxidized. Oxidation of Cys-298 to a sulfenic acid moiety, but not sulfonic or sulfinic acid, could be another possibility for the conversion of the native form of the enzyme to the activated form. Agents such as dithiothrietol, have however, been established to reverse the sulfonic and sulfinic acid forms back to the unoxidized enzyme forms [5]. Further completed works on kinetic studies, utilizing site directed mutagenesis of specific cysteine residues located on the active site of human aldose reductase would in the successive pages provide further insight into the manner in which modification of a key residue leads to modulation of the enzyme activity.

The nature of the activated form of human aldose reductase and the identity of amino acid residues involved in substrate binding and/or catalysis is unknown. Oxidation of human aldose reductase has also been found to result in multiple isoforms, presumably

due to disulfide formation with thiol compounds, which altered the susceptibility to inhibition by inhibitors such as sorbinil [5]. Petrash *et al*., (1992), studied the potential role of several cysteine residues in the catalysis and the inhibition of hAR. Human placental aldose reductase contains six cysteine residues [8], three of which are accessible to solvent and react readily with agents DTNB (5,5'-dithiobis(2-nitrobenzoic acid)). It has further been proposed that oxidation-induced activation of hAR, and changes in the kinetic and inhibitor-binding properties of the enzyme, may be due to modification of one or more of the cysteine residues [6]. *Petrash et al*., (1992), using site-directed mutagenesis, constructed three mutants Cys-298-Ser, Cys-80-Ser, and Cys-303-Ser, in order to understand the involvement of any of the three cysteine residues in the catalysis and inhibition of hAR.

Enzyme kinetics of each of the mutants using various substrates (Table 1.2), demonstrated that of the three mutants, only Cys-298-Ser mutation produced characteristics similar to the activated enzyme form, evident by high V_{max}/K_m, and a lowered sensitivity to a potent inhibitor, sorbinil, but not to the inhibitor, tolrestat.

Table 1.2: Kinetic parameters for wild-type and mutant aldose reductase using different substrates [47]. As reported by Petrash *et al*., (1992)

Parameter	Wild type	C80S	C298S	C303S
D-Xylose				
K'_m(mM)	10.2 ± 1.49	15.6 ± 1.55	543 ± 102[a]	290 ± 36[a]
k_{cat} (s^{-1})	1.24 ± 0.06	1.52 ± 0.04	8.84 ± 0.85[a]	0.81 ± 0.4
k_{cat}/K'_m ($s^{-1}M^{-1}$)	122 ± 13.5	97.6 ± 8.07	15.7 ± 1.52[a]	2.77 ± 0.23[b]
D-Glucose				
K'_m(mM)	212 ± 26.7	196 ± 24	>1000[a]	881 ± 277[a]
k_{cat} (s^{-1})	0.086 ± 0.004	0.359 ± 0.026[a]	>1.95[a]	0.037 ± 0.004[a]
k_{cat}/K'_m ($s^{-1}M^{-1}$)	0.407 ± 0.033	1.87 ± 0.269[a]	ND[b]	0.085 ± 0.010[a]
p-Nitrobenzaldehyde				
K'_m(mM)	15.7 ± 1.70	34.6 ± 6.79	202 ± 14.1[a]	254 ± 20.2[a]
k_{cat} (s^{-1})	0.469 ± 0.011	0.377 ± 0.014[a]	3.33 ± 0.092[a]	0.486 ± 0.016
k_{cat}/K'_m ($s^{-1}M^{-1}$)	29,738 ± 2,689	10,865 ± 1.881[a]	16,432 ± 741[a]	1912 ± 94[a]
Benzaldehyde				
K'_m(mM)	72.8 ± 11.3	27.6 ± 3.49	1,061 ± 208[a]	67.7 ± 36[a]
k_{cat} (s^{-1})	0.443 ± 0.044	0.758 ± 0.018[a]	4.62 ± 0.121[a]	0.299 ± 0.111[a]
k_{cat}/K'_m ($s^{-1}M^{-1}$)	6,093 ± 742	27,473. ± 3,033[a]	4,404 ± 377[a]	4,420 ± 501

[a] $p<0.001$ compared to ALR2:Wild type.

[b] ND, value could not be accurately computed in K'_m and k_{cat} components.

Values of kinetic constants are mean ± S.E (n=15). The indicated substrates are varied over a concentration range of at least 0.1-2 times K'_m. K'_m values are apparent Michaelis constants for the indicated substrate [47]

Table 1.2 shows that the enzyme kinetic constants of the wild type and the mutant reductases were determined by varying the substrates including benzaldehyde, *p*-nitrobenzaldehyde, glucose, and xylose, where each have different polar properties [47]. As evident from the table, the measured k_{cat}/K_m of the mutant enzymes (Cys-298-Ser, Cys-80-Ser and Cys-303-Ser), using substrates such as *p*-Nitrobenzaldehyde (16,423 ± 741) was much greater for a substrate such as glucose, whose k_{cat}/K_m could not be accurately determined because it was exceedingly small [46]. Since hydrophobic residues are located at the active site of the enzyme, there seemed to be more attraction for hydrophobic substrates [47]. The Cys-298-Ser mutant, from Table 1.2, clearly had the greatest differences in substrate specificities when compared to the wild-type. Focusing on the Cys-298-Ser mutant, using glucose, for example as the substrate, the K_m value was remarkably higher than that of the wild-type. The k_{cat} for the Cys-298-Ser mutant, using all the substrates was higher than that of the wild-type. However, the catalytic efficiency (k_{cat}/K_m) of this mutant was lower than that of the wild-type. Using DL-glyceraldehyde (shown in Table 1.3) as the substrate, the turnover number also increased appreciably [47].

Chemical modification studies further distinguish Cys-298-Ser as an important regulatory site of hAR. Table 1.3, as presented below, shows that carboxymethylation of the Cys-298-Ser mutants, unlike the wild-type (ALR:WT), the Cys-80-Ser, and the Cys-303-Ser mutants led to no substantial effect on the kinetic parameters.

Table 1.3 also shows that carboxymethylation of all the mutants and the wild-type, except for the Cys-298-Ser mutant, caused a decrease on the turnover number, hence less time is needed to turn over one molecule of the substrate to the product for the

Cys-298-Ser mutant after carboxymethylation. The very little observed changes following carboxymethylation of the Cys-298-Ser mutant enzyme confirms the Cys-298 residue as the significant site of carboxymethylation of human aldose reductase [47].

Table 1.3. Kinetic parameter of reduced and carboxymethylated wild type and mutant aldose reductase [47]. As reported by Petrash *et al*., (1992)

Parameter	ALR2:WT	C80S	C298S	C303S
Reduced enzyme				
k_{cat}	4.49 ± 0.420	3.34 ± 0.155	15.70 ± 2.108[a]	3.38 ± 0.207
K_m (DL-glyceraldehyde)	0.05 ± 0.003	0.07 ± 0.005	2.71 ± 0.146[a]	0.07 ± 0.002[a]
K_m *(NADPH)*	0.05 ± 0.009	0.06 ± 0.005	0.15 ± 0.029	0.05 ± 0.006
Carboxymethylated enzyme				
k_{cat}	2.73 ± 0.205	2.46 ± 0.134	18.24 ± 2.153[a]	1.83 ± 0.139
K_m (DL-glyceraldehyde)	0.36 ± 0.089	0.38 ± 0.009	2.46 ± 0.257[a]	0.30 ± 0.055[a]
K_m *(NADPH)*	0.05 ± 0.010	0.09 ± 0.009	0.19 ± 0.031	0.05 ± 0.008

[a] $p<0.001$ compared to ALR2:WT (aldose redcutase wild-type).

K_i values are expressed in the micromolar range.

The enzyme was reduced by incubating in 0.1M DTT for 1 hr at 37°C in 0.1M Tris HCl, pH 8.0. Excess DTT was removed by gel filtration. The reduced enzyme were carboxymethylated by incubation with 1mM iodoacetic acid at 23°C for 1 h in 0.1M Tris HCl, pH 8.0. The concentration of DL-glyceraldehyde was varied from 0.1 to 10µM and NADPH from 10 to 100µM. Values of the parameter are mean ± S.E. (n=5). K'_m are apparent values expressed in mM and K_{cat} values in s^{-1}. [47].

Table 1.4 below is a representation of the work of Petrash *et al*., (1992). In further investigating the role of these cysteine residues, these researchers studied the inhibitor sensitivities of the three mutants (Cys-298-Ser, Cys-80-Ser and Cys-303-Ser), using two inhibitors, sorbinil and tolrestat. The carboxymethylated forms of the mutant enzyme forms and the wild type were also studied. From the table, looking at the reduced enzyme form, it is evident that the Cys-298-Ser mutant showed reduced sensitivity to an otherwise potent inhibitor like sorbinil, when compared to the wild-type, as a large increase was depicted for the K_i of the Cys-298-Ser. Hence the regulatory role of the Cys-298 residue in the functioning of human aldose reductase and the reiterated insensitivity to the activated form of the enzyme. The sensitivity to tolrestat of the reduced form of the three mutants was not greatly affected as shown on Table 1.4. Therefore, the Cys-298 residue of human aldose reductase has no effect on tolrestat binding.

Table 1.4: Inhibitor sensitivity of the reduced and carboxymethylated aldose reductase [47]. As reported by Petrash *et al*., (1992)

Parameter	ALR2: WT	C80S	C298S	C303S
Reduced enzyme				
$K_{i\ (sorbinil)}$	0.37 ± 0.023	0.84 ± 005[a]	3.81 ± 0.18[a]	0.55 ± 0.057
$K_{i\ (tolrestat)}$	0.015 ± 0.002	0.022 ± 0.002	0.015 ± 0.002	0.042 ± 0.011
Carboxymethylated enzyme				
$K_{i\ (sorbinil)}$	>50	>150	4.10±0.26	>100
$K_{i\ (tolrestat)}$	0.038 ± 0.007	0.428 ± 0.086[a]	0.015 ± 0.002	0.053 ± 0.017

[a] $p<0.001$ compared to ALR2:WT.

K_i values are expressed in the micro molar range.

The concentration of DL-glyceraldehyde was varied from 0.1 to 10mM. The concentration of sorbinil was varied from 0.01 to 10μM for the reduced enzyme and from 1 to 150μM for the carboxymethylated enzyme. The concentration of tolrestat was varied from 0.0025 to 0.1μM. Values of the parameter are mean ± S.E. (n=5) [47].

Carboxymethylation was used as a chemical modification to again study the functionality of the Cys-298 residue. Compared to the reduced enzyme form, carboxymethylation had no effect on the K_i values of the mutant Cys-298-Ser for sorbinil, but a dramatic effect was seen for the other two mutants and the wild-type enzyme form [47]. Using tolrestat, the K_i value of Cys-298-Ser mutant also had no increase or decrease after carboxymethylation. The result of this section of the research reinforces that the functionally significant site of carboxymethylation in aldose reductase is Cys-298, and that this residue is significantly important in the modulation of inhibitor sensitivity [47].

The crystal structure pig lens aldose reductase have three cysteine residues– Cys-80, Cys-298 and Cys-303, located on the C-terminal region of the β/α-barrel motif [56]. There exists a great sequence similarity between the structure of the pig lens aldose reductase and hAR [47], suggesting the likelihood for the similarity of the structures for studies, in comparison to each other. Only Cys-298 is located in a favorable distance (within 4.13Å) of the C-4 of the nicotinamide portion of NADPH when complexed with human aldose reductase. This portion is considered to be the active site of the enzyme. Hence Cys-298 is located in proper proximity to affect both enzyme activity and inhibitor sensitivity. From the work of Petrash *et al*., (1992); it could also be deduced that Cys-298, in contrast to His-110, as explained earlier, could not be the proton donor in the overall catalysis, since the substitution of the thiol group in Cys-298 with a hydroxyl group in serine, has little effect on the catalytic activity, but could also modify the interaction of the side chains with the nicotinamide ring.

Overall, based on the work of Petrash *et al*., (1992), and the accumulating body of evidence presented in the Tables (1.2, 1.3, and 1.4) above explained at that time that none of the three residues (Cys-298-Ser, Cys-80-Ser, or Cys-303-Ser) were essential for catalysis, but rather the Cys-298-Ser mutant was well established to be involved in inhibitor sensitivity including other properties like carboxymethylation. The kinetic parameters of the Cys-298-Ser mutant (as shown in Table 1.4) are incomparable to those of the wild-type, Cys-80-Ser or the Cys-303-Ser mutants, hence the important role of the Cys-298 residue in the enzyme.

Increased turnover rate (k_{cat}), facilitated by $NADP^+$ release, is presumed to result from the activation of aldose reductase and from the isomerization rate of the E•$NADP^+$ binary complex [5], [39]. Hence if activation is due to oxidation of one of the cysteine residues, modification of these residues should lead to a k_{cat} increase, evident on only the Cys-298-Ser mutant.

Cappiello *et al*., (1996) [15], observed the modification of human aldose reductase by physiological disulfides. Their observation recapitulates another key characteristic of the Cys-298 residue. They demonstrated that the Cys-298 residue is the principal site of thiolation of human aldose reductase. These researchers examined the rate of enzyme inactivation using wild-type human aldose reductase, Cys-80-Ser, Cys-298-Ser, and Cys-303-Ser mutants. Using glutathione disulfide (GSSG) and cystine, these researchers incubated the wild-type, Cys-298-Ser, Cys-80-Ser, and Cys-303-Ser mutants. The results showed a tremendous loss of activity for all enzyme forms, except the Cys-298-Ser mutant. This loss of activity corresponded with thiolation of human aldose reductase and reiterates the fact the oxidation of the enzyme brought about by Cys-298 is the target residue for post-translational modification [15]. $NADP^+$ was also known to shield all the mutants from GSSG-induced inactivation, except for the Cys-298-Ser mutant, which remained insensitive to inactivation regardless of the presence of $NADP^+$[15]. This result corroborates other findings that have been reported by other researchers, such as Vander Jagt *et al*., 1990, on the modification of aldose reductase by several agents and the protection offered by oxidized NADPH. Therefore, the Cys-298 residue is thought to be the only residue that is sufficiently close to $NADP^+$ to be shielded

from modification, and this residue's interaction with $NADP^+$ affects the sensitivity of the enzyme to inhibition by agents like cystine and GSSG [15].

In addition to the results of the work of Capiello *et al*., (1996), their findings also indicated that Cys-298 is an essential site of regulation on hAR in which inactivation by physiological disulfides [15], or menadione [7], and activation by DTT (dithidiethanol) [7], [15] is focused on the Cys-298 residue. Research has shown that the thiolation of Cys-298 is responsible for the conversion of human aldose reductase to the activated form and that thiolation produces characteristics of the activated enzyme – evident by insensitivity to inhibitors. In support of this, inactivation of cardiac aldose reductase by HNE (4-hydroxynonenal) is believed to be due to the modification of Cys-298, because the modification of Cys-298 of placental aldose reductase or the site directed mutagenesis of Cys-298 to Ser-298 leads to similar differences observed with HNE modified enzymes [63].

Balendiran *et al*., (2011), evaluated how site-directed mutagenesis may elucidate the features of activated human aldose reductase, using the Cys-298-Ser mutant. This mutant had been identified as important and regulatory to aldose reductase function. In addition, Balendiran *et al*, (2011), sought to understand the substrate specificity of the Cys-298-Ser mutant and the wild-type with more substrates than had been earlier reported by other researchers. The substrates utilized for the aldehyde reduction kinetics of the mutant and the wild-type were DL-glyceraldehyde, D-glucose, and 4-hydroxynonenal, while for the alcohol oxidation kinetics, benzyl alcohol was the only substrate used.

Using D-glucose and HNE (as shown in Table 1.5), the turnover number reduced significantly indicating that it would require more time to turn over one molecule of these substrates to products by the mutant (Cys-298-Ser) when compared to the wild-type [1], however, using DL-glyceraldehyde, the turnover number, k_{cat} for the mutant, increased compared to the wild-type. A look at the catalytic efficiencies (k_{cat}/K_m) of the Cys-298-Ser mutant showed that there was an inconsistent reduction with each of the substrates used. Benzyl alcohol is the only substrate for the reverse reaction; the K_m value for Cys-298-Ser was appreciably higher also. The overall trend for the affinity was attributed to the strength of the enzyme-substrate complex for the forward and the reverse reaction being weakened for the Cys-298-Ser mutant, compared to the wild-type enzyme [1].

Table 1.5: Comparison of the catalytic activity of the wild-type and the Cys-298-Ser mutant hAR for carbonyl reduction and alcohol oxidation reactions at 25°C [1]. As reported by Balendiran *et al*., (2011).

The uncertainties are S.D. of the average value

hAR Protein	**Substrate**	K_m	K_{cat}	K_{cat}/K_m
Wild-type	DL-glyceraldehyde	0.1 ± 0.01 mM	1.55 ± 0.01	14.5 $mM^{-1}s^{-1}$
Cys-298-Ser		1.2 ± 0.05 mM	3.72 ± 0.3	3.10 $mM^{-1}s^{-1}$
Wild-type	D-Glucose	55.0 ± 6.0 mM	0.64 ± 0.05	0.01 $mM^{-1}s^{-1}$
Cys-298-Ser		800 ± 50.0 mM	0.42 ± 0.04	0.0005 $mM^{-1}s^{-1}$
Wild-type	HNE	48.0 ± 4.0 μM	0.90 ± 0.06	0.019 $\mu M^{-1}s^{-1}$
Cys-298-Ser		110.0 ± 8.0μM	0.60 ± 0.02	0.006 $\mu M^{-1}s^{-1}$
Wild-type	Benzyl alcohol	1.62 ± 0.1mM	0.35 ± 0.025	0.215 $mM^{-1}s^{-1}$
Cys-298-Ser		4.55 ± 0.3mM	0.42 ± 0.02	0.092 $mM^{-1}s^{-1}$

From the results of the work of Balendiran *et al*, (2011), shown above, the K_m for each of the mutants, utilizing all substrates also increased compared to the wild-type. These findings were consistent with those observed for the activated form of the enzyme, and with previous results reported by other researchers. These studies support the hypothesis that residue Cys-298 is an important regulatory residue, and is key to the conversion of native human aldose reductase to the activated form – inhibitor-insensitive enzyme form (up to a 1000-fold insensitivity).

Evidence in support of the study by Balendiran *et al*., (2011), was resolved better by comparison of the structure wild-type and the Cys-298-Ser mutant human aldose reductase complexed with $NADP^+$, as shown in Figure 1.4 and Figure 1.5 [1]. The side chain of Cys-298 from Figure 1.4 in the wild type is surrounded by hydrophobic residues, such as Trp-20, Tyr-209 and Trp-219, and the nicotinamide ring of NADPH, and is about 5 Å from these residues [1].

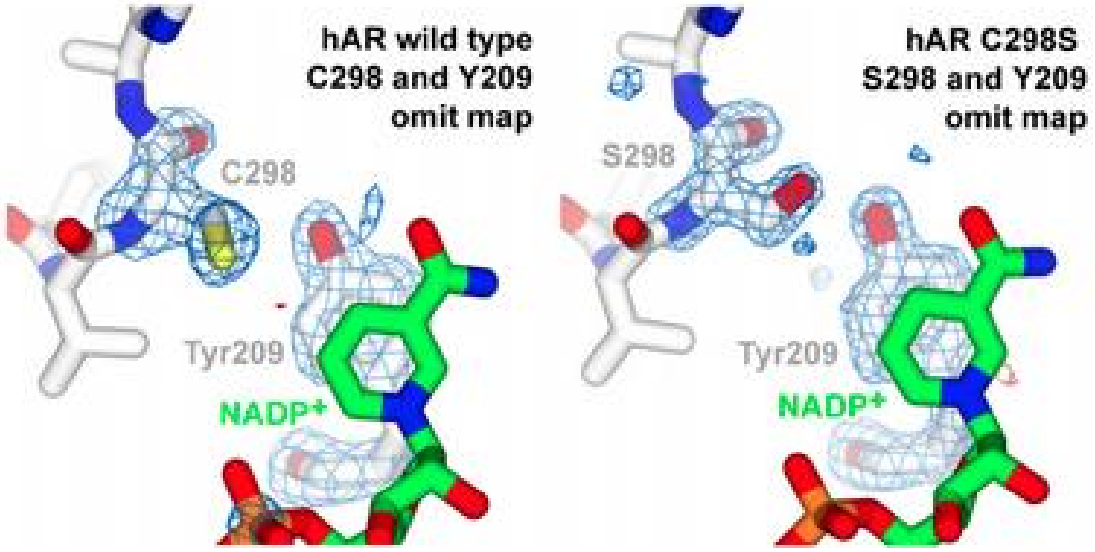

Figure 1.4: Omip Map corresponding to Tyr-209 in the wild-type and C298S mutant hAR. Omit maps of wild-type and C298S mutant hAR corresponding to the omitted regions of the residue 298 and 209 are shown. The maps are calculated with CNS simulated algorithm of the coordinates without the residues 298 and 209, and $F_o - F_c$ omit maps are contoured at ± 4σ [1].

Figure 1.5 shows the superposition of the wild-type hAR and the Cys-298-Ser mutant enzyme. This explains in details the interaction of the Cys-298 residue of the wild-type, and the Ser-298 residue of the mutant, with the hydrophobic Tyr-209 residue, and the nicotinamide ring of $NADP^+$. From Figure 1.4 and Figure 1.5, residue Cys-298 of the wild-type forms van der Waals' interactions with the C5 and C4 of the nicotinamide ring [1], and no hydrogen bond exists. The Ser-298 residue of the mutant however, forms a hydrogen bond between the hydroxyl group of serine and the hydroxyl group of Tyr-209 (Figure 1.5), therefore making the side chain of the Cys-298-Ser mutant less flexible [1]. The reduced flexibility of the Ser-298 residue of the mutant enzyme explains the reduced binding affinity that is shown in Table 1.5 as the increased K_m for various substrates of the Cys-298-Ser mutant enzyme.

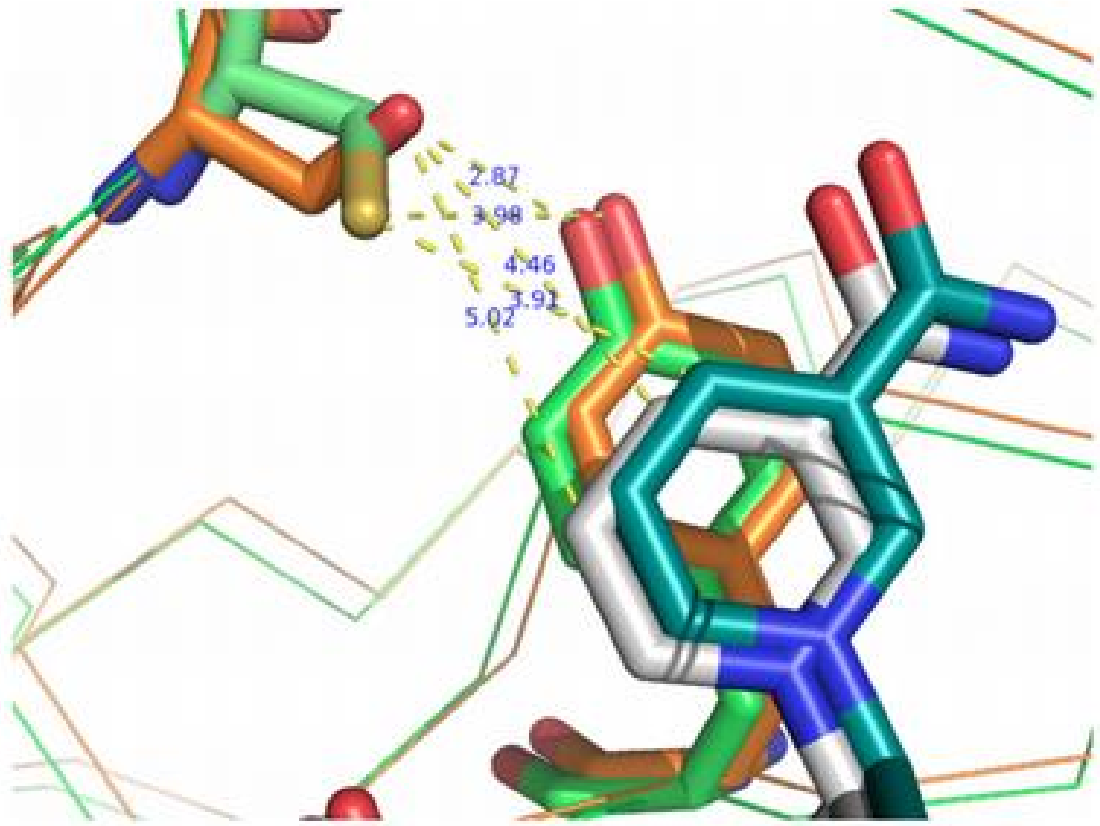

Figure 1.5. Superposition of wild-type (brown) and Cys-298-Ser (green) hAR. The side chain of residues Cys-298 (*green*), Ser-298 (*brown*), and their interaction with residue Tyr-209 and nicotinamide ring of $NADP^+$ in the wild-type and Cys-298-Ser mutant hAR are shown [1].

As a further consequence of the mutation with regards to the binding of NADPH comparative to $NADP^+$, as reported by the researchers, the polarity of the mutated Ser-298 side chain is likely to be less compatible with the NADPH complex compared with the $NADP^+$ [1]. The increase in polarity brought about the mutation to serine destabilizes the NADPH binding, but not $NADP^+$. This increase in the polarity of the nicotinamide, and the reduced affinity for all the substrates explains the decrease in the

strength of the interaction of the Cys-298-Ser mutant with the various substrates compared to the wild-type. These factors taken as a whole and the kinetic properties for the wild-type and the Cys-298-Ser mutant, very similar to those evaluated by previous researchers, explains the importance of the Cys-298 residue as important in the cofactor binding, conformational rearrangement and inhibition of human aldose reductase.

1.5.1 Oxidative Post-Translational Modification of Cysteine

As stated earlier, oxidation of cysteine residues in aldose reductase affects catalysis, substrate specificities, and inhibitor binding [47]. Much effort has been put into research in understanding that the oxidation of Cys-298 is a physiological process and could be induced by some species and compounds such as nitric oxide (NO) and reactive oxygen species. Cys-298 has been identified as located on the active site of aldose reductase [47]. Interactions between Cys-298-Ser and NADPH appear to determine the rate of isomerization of the E•NADP$^+$ binary complex, and the decrease in k_{cat} of the residue and the cofactor binding may be due to slower isomerization of the E•NADP$^+$ binary complex [6]. Oxidation of Cys-298 in aldose reductase inhibits the complete closure of the NADPH-binding loop, making the binding loop easier to open during NADP$^+$ release; this step is the rate-limiting step in the catalysis of aldose reductase. Increased NADP$^+$ release therefore correlates with increased k_{cat}. Based on these assumptions, Cys-298 residue of aldose reductase, more like the specific cysteine residue in other proteins has been proposed to be nitrosylated, glutathionylated or oxidized to sulfenic, sulfinic and sulfonic acid [35], [60], [49]. These alterations have been displayed

in certain mutants like the Cys-298-Ser mutant, w hich produces similar characteristics to the oxidized (activated) enzymes.

The availability of different oxidation states of sulfur in most proteins permits the formation of a diverse range of oxidative post-transformational modifications, brought about by reactive oxygen species or reactive nitrogen species. These modifications include disulfide bonds formation (RS-SR'), sulfinic acid (SO_2H), sulfonic acid (SO_3H), S-nitrosylation (SNO), sulfhydration (SSH), S-glutathionylation (RS-SG), and sulfenylation (SOH). Although, the formation of oxidative post transformational modifications depends on certain factors like the composition of local redox environment, the reactivity of individual cysteine residue and its surrounding environment [30], the underlying mechanism in which oxidative post-translational modification occurs in aldose reductase remains unclear, but is believed to result from the oxidation of a cysteine residue, most significantly Cys-298.

Activation of human aldose reductase by reactive oxygen species, brought about by oxidation of its cysteine residues to sulfenic acid in ischemic heart have been reported [35]. Recent findings also have shown that nitric oxide activates aldose reductase in ischemic hearts, which is attributed to peroxynitrite-mediated oxidation of Cys-298 to sulfenic acid via the P13K/Akt/endothelial NOS pathway [36].

1.3 Objective of Thesis

The Cys-298 residue has been established as an important residue to undergo modifications in the study of aldose reductase. The modification to this residue has been successful in understanding to an extent, and from a biological standpoint, the *in vitro* processes which is thought to occur in various organisms, especially in humans.

The objective of this thesis is divided into three focuses:

1. **To produce two mutants (Cys-298-Asn and Cys-298-Glu):** The mutant extensively studied in understanding the mechanism of aldose reductase function is the Cys-298-Ser mutant, which produces characteristics that are similar to activated (oxidized) aldose reductase. The Cys-298-Ser mutant differs from the wild-type aldose reductase by the replacement of a sulfur atom with an oxygen atom. The discrepancies in the properties of the residues result in large differences in properties such as the pK_a value. This thesis explores the mutants (Asn-298), a polar uncharged amino acid, which differs from a cysteine by the replacement of a thiol group with a carboxyamide group, and Glu-298, an acidic amino acid, which differs from cysteine by the replacement of a thiol with a carboxyethyl group.
2. **To analyze the effect of these mutations on Cys-298 using enzyme kinetics:** Following successful production of these two mutants, enzyme kinetics would be performed in studying the activity of the mutants with several substrates and cofactors, with the rates analyzed according to the Michaelis-Menten model.
3. **To delineate the significance of the Cys-298 residue in catalysis:** The results of this thesis following mutants' synthesis and characterization using enzyme

kinetics, may be effective in explaining the characteristic of Cys-298 residue in catalysis, and its direct involvement in oxidation of hAR.

2.0 Materials and Methods

2.1 Materials

QuickChange II Site-Directed Mutagenesis Kit containing XL1-Blue supercompetent *E.coli* cell and BL21 (DE3) competent *E.coli* was obtained from Agilent Technologies, Santa Clara, CA; 2-mercaptoethanol obtained from Amresco Inc., Solon, OH; Difco yeast extract, Ultrafiltered, Bacto Agar, Bacto Tryptone, Sodium Chloride, Disposable Culture Tubes and 10mL, 20mL and 3mL syringes were obtained from BD Biosciences, San Jose, CA; J.T. Baker Sodium Hydroxide pellets, J.T. Baker Ammonium persulfate (Baker analyzed A.C.S Reagent), magnesium chloride, sodium hydrogen phosphate, potassium dihydrogen phosphtate were obtained from Avantor Performance Materials Inc., Centre Valley, PA; Millex-GV Syringe Filter Unit (0.22uM), Millex-HV Syringe Filter Unit (0.45uM), Novagen 4x SDS sample buffer, Novagen pET 15b-DNA were obtained from EMD Millipore, Darmstadt, Germany; Ultra-Pure Isopropyl-β-D-Thiogalactopyranoside (IPTG) was obtained from Biopioneer Inc., San Diego, CA. QIAPrep Spin Miniprep Kit and TE buffer was obtained from Qiagen, Venlo, Netherlands; 1,3 – Diaza-2, 4-cyclopentadiene (Imidazole), 4-morphonlineethansulfonic acid, Trizma (Tris (hydroxymethyl)aminomethane Base (Sigma 7-9), DL-glyceraldehyde, D-glucose, NADPH, benzylalcohol, HEPES, Luria Broth (Miller) were obtained from Sigma-Aldrich Corporation, St. Louis, MO; Acrylamide/Bisacrylamide (N, N- Methylene bisacrylamide) liquid (37.5:1) was obtained from Roche Diagnostic Corporation, Indianapolis, IN; Spectra/Por Molecularporous membrane tubing (dialysis tubing) 6-8k MWCO, 23mm flat width, 100ft was obtained from Spectrum Laboratories inc., Rancho

Dominguez, CA; Coomassie Brilliant Blue G-250, Sodium Dodecyl Sulfate Electrophoresis purity Reagent, Tetramethylenethylenediamine (TEMED), Bromophenol Blue, Protein Standard I Globulin (bovine y-globulin), Resolving Gel Buffer (1.5M Tris-HCl pH 8.8) Stacking Gel buffer (0.5M Tris–HCl pH 6.8), 10x Tris/Glycine/SDS Electrophoretic buffer, Quick Start Bradford 1x Dye Reagent, Quick Start ^{TM} Bovine Serum Albumin (BSA) Standard was purchased from Bio-Rad Laboratories Inc., Hercules, CA; Clontech TALON CellThru (IMAC) resin was purchased from Clontech Laboratories Inc., Mountain View, CA; Magnesium sulfate, potassium chloride, Falcon 15mL conical centrifuge tubes, 50mL graduated polypropylene centrifuge tubes, glycerol PageRuler Plus Prestained Protein Ladder, glucose were obtained from Thermo Scientific Inc., Waltham, MA; ethyl alcohol (190 proof), hydrochloric acid, acetic acid and absolute methanol were obtained from Pharmco-Aaper, Toronto, Canada.

2.2 Buffers, Strains and Media

The QuickChange II site-directed mutagenesis kit as earlier mentioned above obtained from Agilent Technologies contained XL1-Blue Supercompetent *E.coli* cell strain. The supercompetent *E.coli* cell strain was utilized in the entire experiment involving the pET-15b vector, the 4.5-kb mutagenesis control plasmid (pWhitescript), and the transformation control plasmid (pUC18). Cells in the experiments were cultured in Luria bertani Broth (0.5% Difco Yeast Extract, 1% NaCl, and 1% Bacto Tryptone) containing 100μg/mL of ampicillin. For the mutagenesis and the transformation control, cells were spread on Luria Bertani Broth-ampicillin (LB-Amp) plates containing 80mg/mL of 5-bromo-4-chloro-3-indoyl-b-D-galactopyranoside (Xgal) and 20mM of

IPTG. Transformants were selected on sterile plates containing Luria Bertani Broth comprising 0.9% of Agar and 100μg/mL of ampicillin. Blue-white screening was achieved with 40μL of 100mM IPTG and 40μL of 40mg/mL X-gal spread on LB-Amp plates. BL21 (DE3) competent *E.coli* cells were cultured in 2X YT Broth, containing 1.6% Bacto Tryptone, 0.5% Difco Yeast Extract and 1% NaCl. SOC media comprising of 4mM KCl, 10mM $MgCl_2$, 10mM NaCl, 10mM $MgSO_4$, 20mM glucose, 2% Bacto Tryptone, 0.5% Difco yeast extract was used in regenerating the heat pulsed cells during XLI-Blue supercompetent cells transformation. Transformants were selected on LB-Amp plates. To achieve the overexpression, successful BL21 (DE3) transformants were grown in 2X YT media containing 100μg/mL of ampicillin (YT-Amp) in Erlenmeyer flasks. Protein expression was induced by supplementing 1mM of Isopropyl-1-thio-b-D-galactopyranoside in the culture medium.

The protein purification buffers used were comprised of extraction buffer (50mM Tris, (pH 7.0) with 3M NaCl and 2mM 2-mercaptoethanol), the elution buffer comprised of 300mM imidazole in 50mM Tris buffer (pH 7.0), with 300mM NaCl and 2mM 2-mercaptoethanol; wash one buffer comprised of 50mM Tris buffer (pH 7.0), with 300mM NaCl and 2mM of 2-mercaptoethanol; wash two buffer comprised of 10mM imidazole in 50mM Tris buffer (pH 7.0), with 300mM NaCl and 2mM of 2-mercaptoethanol.

The protein dialysis buffer contained 50mM Tris buffer (pH 7.0), with 300mM NaCl and 2mM of 2-mercaptoethanol. The staining solution used for staining the SDS-PAGE gel after running the protein samples was made up of 50% methanol, 10% acetic acid, 40% water and 0.3% Coomassie Brilliant Blue G-250. The destaining solution was made up of 10% acetic acid, 60% water and 30% methanol. The gel running buffer was

composed of 1x Tris/Glycine/SDS Electrophoresis buffer (25mM Tris, 192mM Glycine and 0.1%SDS, pH 8.3). The 1x phosphate buffered saline was prepared with 0.024% potassium diphosphate, 0.144% sodium phosphate, 0.02% KCl, 0.8% NaCl (pH 7.4). The 4x SDS protein sample buffer was made with 5% BME, 240mM Tris (pH 6.8), 40% glycerol, 8% SDS, and 0.04% bromophenol blue. The 2x SDS protein sample buffer was made by diluting the 4x SDS protein sample buffer with 1x PBS buffer.

2.2.1 pET 15b Vector

The bacterial expression vector used for the purpose of the study was the pET 15b vector. This vector in which the mutant framework was designed across contains an N-terminal His•Tag® sequence as shown below, an ampicillin resistance gene, allowing for the selection of recombinants, a thrombin cleavage site and three cloning sites (multiple cloning site). Unique sites on the pET 15b vector are shown on the circular map shown in Figure 2.1. It is important to note that the T7 expression region is reversed on the circular map. The coding/expression region transcribed by the circular strand is also shown below the map.

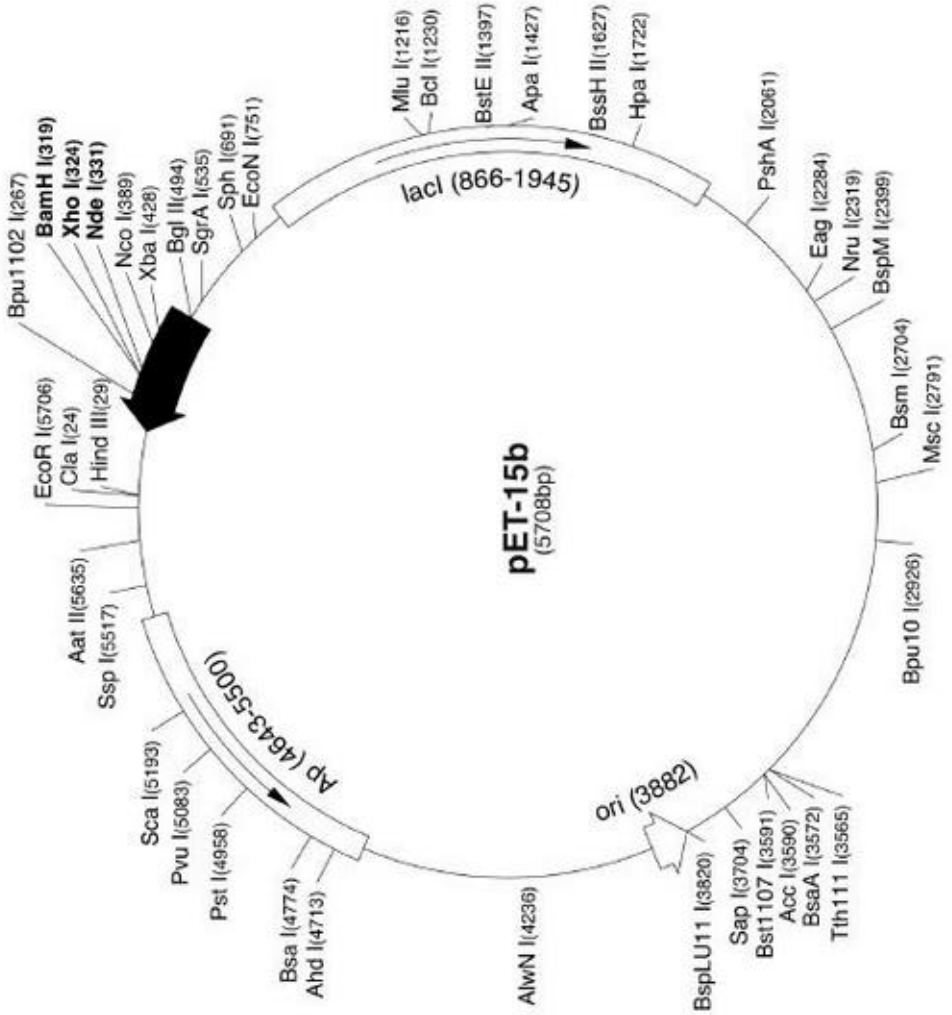

pET-15b sequence landmarks	
T7 promoter	463-479
T7 transcription start	452
His•Tag coding sequence	362-380
Multiple cloning sites (*Nde* I - *Bam* H I)	319-335
T7 terminator	213-259
lacI coding sequence	(866-1945)
pBR322 origin	3882
bla coding sequence	4643-5500

Figure 2.1. Map of pET-15b vector. Figure adapted from www.agilent.com

2.2.2 pWhitescript

pWhitescript control plasmid is contained within the mutagenesis kit. The pWhitescript™ 4.5-kb control plasmid is used to test the efficiency of mutant plasmid generation using the QuikChange II site-directed mutagenesis kit. The pWhitescript 4.5-kb control plasmid contains a stop codon (TAA) at the position where a glutamine codon (CAA) would normally appear in the β-galactosidase gene of the pBluescript® II SK(–) phagemid. XL1-Blue supercompetent cells transformed with this control plasmid appear white on LB–ampicillin agar plates containing IPTG and X-gal, because β-galactosidase activity has been interrupted. A point mutation is created on the pWhitescript 4.5-kb control plasmid that reverts the T residue of the stop codon (TAA) at amino acid 9 of the β-galactosidase gene to a C residue to produce the glutamine codon (CAA) found in the wild-type sequence. Following transformation, colonies can be screened for the β-galactosidase (β-gal+) phenotype of blue color on media containing IPTG and X-gal.

2.2.3 pUC18

The artificial plasmid pUC18 has been genetically engineered to include a gene for antibiotic resistance to Ampicillin (amp^R), multiple cloning site (MCS), and a gene for the enzyme beta-galactosidase (*lacZ*). The *lacZ* gene contains a polylinker region, with a series of unique restriction sites found nowhere else in the plasmid.

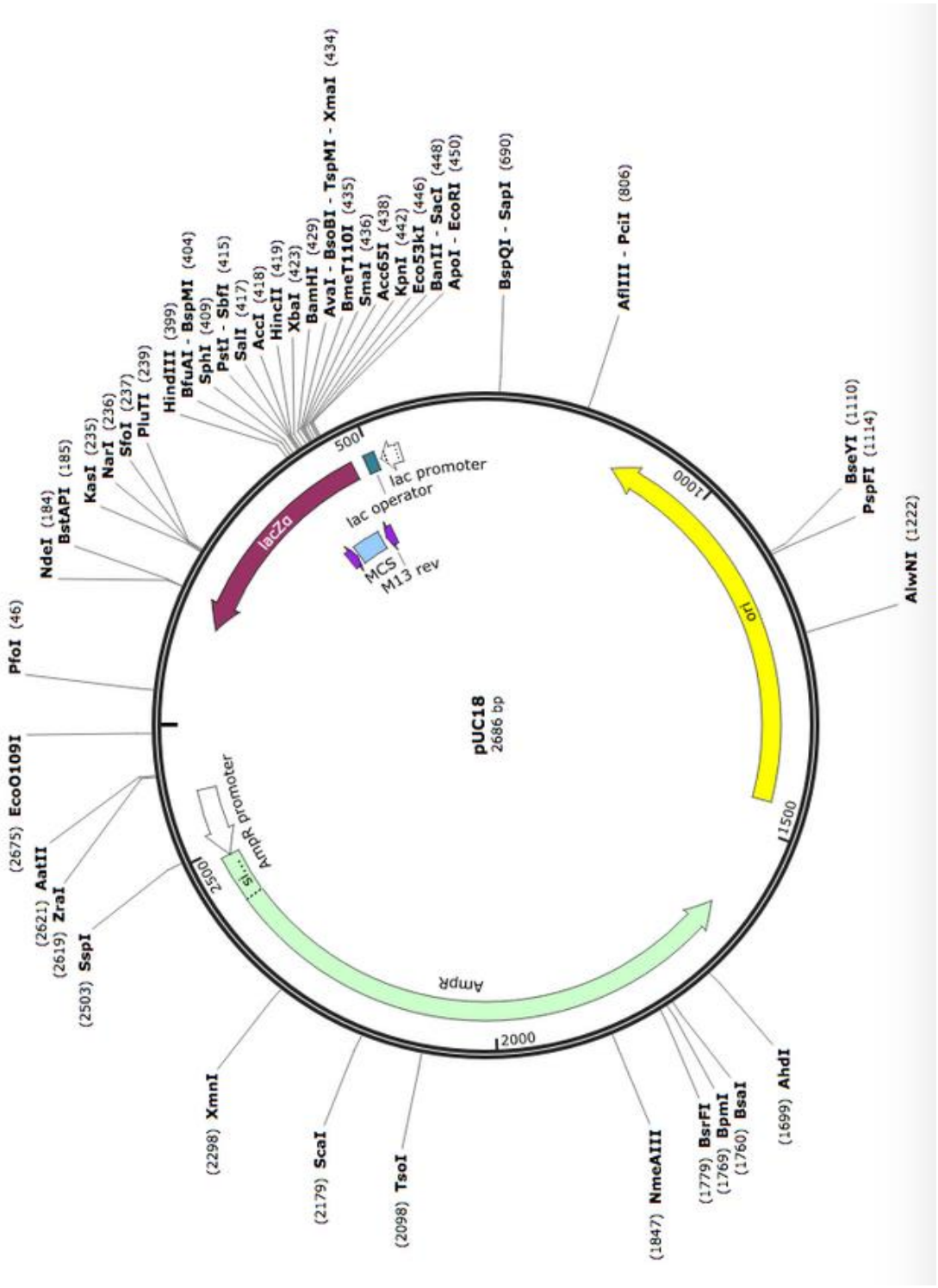

Figure 2.2: Restriction map of the transformation control plasmid (pUC18). Enzyme cleavage sites are shown at the restriction location on the control plasmid. Figure adapted from www.snapgene.com.

2.3 Methods

2.3.1 Mutagenic Primer Designs

Mutagenic primers were designed using the web-based QuickChange Primer Design Program on www.agilent.com/genomics/qcpd. The desired mutation is in the middle of the primer with ~10-15 bases of the correct sequence on both sides, flanked by unmodified nucleotide sequence. The primer design was made to incorporate a GC content of about 40%, 25-45 total bases in length of the entire oligonucleotide chain length.

2.3.2 Polymerase Chain Reaction

Following mutagenic primer synthesis, polymerase chain reaction was performed in a thermocycler, using various specifics in temperature regulation. For each mutant that was synthesized, varying melting temperatures were used to accommodate the desired mutation. Two mutations were created for the Cys-298 residue of *hAR* to Cys-298-Asn (Cysteine residue mutated to asparagine) and Cys-298-Glu (cysteine mutated to glutamate). The following complementary oligonucleotide primers shown in Table 2.1 were synthesized for the mutagenesis protocol and highlighted in red is the effected mutation. The percentage GC content and the melting temperatures are also specified below.

Table 2.1: Mutagenic primers sequences, melting temperature and percentage GC content.

Primer	Mutant	Sequence 5' to 3'	Tm (°C)	%GC Content
Forward	Cys-298-Glu	CAACAGGAACTGGAGGGTC**GAG**G CCTTGTTGAGCTGTACCT	75.7	56.1
Reverse	Cys-298-Glu	AGGTACAGCTCAACAAGGC**CTC**G ACCCTCCAGTTCCTGTTG	75.7	53.7
Forward	Cys-298-Asn	CAACAGGAACTGGAGGGTC**AAC**G CCTTGTTGAGCTGTACCT	74.7	53.7
Reverse	Cys-298-Asn	AGGTACAGCTCAACAAGGC**GTT**G ACCCTCCAGTTCCTGTTG	74.7	53.7

After primer design, the following reagents were mixed for the sample reaction and the control reactions to take place, for a total volume of 50µL, with a constant primer concentration.

Table 2.2: Mutagenesis sample reaction composition.

Reagents Used	Volume (μL)
10x reaction buffer	5
5ng/μL of *hAR* dsDNA template	3
10μM of oligonucleotide forward primer	1.25
10μM of oligonucleotide reverse primer	1.25
dNTP mix	1
ddH_2O	37.5
PfuUltra High-Fidelity DNA polymerase (2.5U/μL)	1

Table 2.3: Mutagenesis control reaction composition.

Reagents	Volume (μL)
10x reaction buffer	5
5ng/uL of pWhitescript 4.5-kb control plasmid	3
10μM of oligonucleotide control forward primer	1.25
10μM of oligonucleotide control reverse primer	1.25
dNTP mix	1
ddH_2O	37.5μL

Consequent to setting up the mutagenesis control reaction and the mutagenesis sample reactions, the tubes containing the reagents were cycled in a thermocycler using the cycling parameter outlined in the Table 2.4.

Table 2.4: Polymerase chain reaction cycling parameters for the QucikChange II Site-directed Mutagenesis.

Segments	Cycle	Temperature (°C)	Time (mins)
1	1	95	0.5
2	25	95 55 68	0.5 1
3	1	4	2

2.3.3 *DpnI* Digestion of the Amplification products.

Following the mutagenesis reaction, the PCR product is digested with *DpnI*. This digestion is crucial, as it cleaves the methylated dsDNA template leaving the mutated DNA. Without the *DpnI* digestion, a large number of the product would be parental. A 1uL of the *DpnI* restriction enzyme (10U/μL) was added to each sample of the control and the mutant amplification solution to digest the methylated, non-mutated supercoil dsDNA. The amplification reaction was mixed gently and thoroughly by pipetting the solution up and down several times, spun down in a microcentrifuge for 1 minute and incubated immediately for 1 hour at 37°C. The digested DNA was then stored at -20°C.

2.3.4 Preparation of Competent cells by Calcium Chloride Treatment.

Chemical treatment of BL21 (DE3) cells and XL1-Blue cells with calcium ions to make the cells competent was achieved chemically by creating pores in the bacterial cells through exposure to high calcium concentration. This makes the cells permeable to DNA. Using a sterile loop, frozen glycerol stock of bacterial cells are inoculated in 100mL of LB-Amp. The cells were grown in a 37°C shaker at 200 rpm to an OD_{600} of 0.4-0.6. As the cells reach this absorbance, the culture was then chilled for about 20-30 minutes, swirling occasionally to ensure even cooling. The cell culture was then transferred into a 50mL centrifuge tube harvested by centrifugation at 5,000 rpm and 4°C for 10 minutes. The supernatant was decanted and the pellets were resuspended in 35mL of ice-cold 0.1M $CaCl_2$ solution. The suspension was placed on ice for 20 minutes. The mixture was again centrifuged at 5,000 rpm, and 4°C for 10 minutes and the resultant pellets resuspended in 1.5mL of ice-cold solution of 0.1M $CaCl_2$ / 40% glycerol. The cell culture was then frozen at -80°C to prevent loss of their efficiency.

2.3.5 Transformation of XL1-Blue supercompetent cells.

The XLI-Blue cells that have been made supercompetent are gently thawed on ice. About 50μL of the supercompetent cells were aliquoted into three prechilled 1.5mL microcentrifuge tubes, representing the control, sample and transformation control reaction tubes. A 5μL volume of the *DpnI* – treated DNA from each control and sample reaction was transferred to the aliquots of the supercompetent cells. As a control, the

transformation efficiency of the XLI-Blue supercompetent cells was verified by transferring a 1μL of the pUC18 control plasmid (0.1ng/μL) into a 50μL aliquot of the supercompetent cells. The three tubes were swirled gently to mix and then incubated on ice for 30 minutes. The tubes for the transformation reactions were heat pulsed for 45 seconds at 42°C, and then the reaction was placed on ice for 2 minutes. About 500μL of the SOC media, preheated to 42°C was added to each transformation reaction tubes and incubated at 37°C for 1 hour with shaking at 200 rpm. The mixtures containing the solution were plated on LB-Ampicillin plates containing IPTG and X-Gal in several volume: 50μL of pUC18 transformation control, 200μL of the pWhitescript mutagenesis control and 250μL of the mutagenesis sample reaction. The transformation plates were then incubated at 37°C for over 16 hours. For the transformation control plates, blue colonies should appear on LB-Amp plates containing IPTG and X-Gal, while the sample mutagenesis reaction plates should produce white colonies with LB-Amp plates containing IPTG and X-Gal.

2.3.6 Plasmid Isolation using QIAprep® Spin Miniprep Kit.

Colonies from successful transformation of the sample mutagenesis reaction were selected and streaked on an LB-Ampicillin plate divided into 6 sections. Colonies were selected and inoculated into a 5mL LB-Ampicillin plate, incubated at 37°C and left to shake overnight. About 1.33mL of the bacterial overnight culture for each mutant sample transformation reaction was dispensed into three, 1.5mL microcentrifuge tubes. The three tubes for each mutant were centrifuged at 8,000 rpm for 3 minutes at room temperature

(25°C). The pelleted bacterial cells were resuspended in 250μL Buffer P1 and then transferred to a microcentrifuge tube. About 250μL of Buffer P2 was mixed thoroughly into the two-microcentrifuge tubes (containing the two sample mutagenesis reaction), and inverted six times until the solution became clear. About 350μL of Buffer N3 was then added to the tube and mixed immediately by inverting the tube 6 times. The resultant solution was centrifuged at 13,000 rpm (~17,900 x g) for 10 minutes at 25°C. The supernatant from the centrifugation was applied to a QIAprep spin column using a pipette and centrifuged for 60 seconds, and the flow through was discarded. The QIAprep spin column was washed by adding 500μL of Buffer PB into the column, centrifuged for 60 seconds and then the flow through was discarded. About 750μL of Buffer PE was again used to wash the QIAprep spin column, and centrifuged for 60 seconds, and the flow through was discarded. Residual wash buffer was removed by an additional centrifugation for 60 seconds. The QIAprep spin column was placed in a 1.5mL microcentrifuge collection tube. The DNA was eluted by adding 50μL of Buffer EB (0.01M Tris·Cl, pH 8.5) to the center of the QIAprep spin column, let to stand for 60 seconds and then centrifuged for 60 seconds. The DNA isolated from this procedure was then stored at -20°C.

2.3.7 DNA Sequencing

In order to verify that the desired mutation was incorporated, DNA sequencing was performed. The 6 tubes of DNA, following the isolation prep were sent for sequencing by Eurofin genomics. The biological sequence editor, BioEdit Sequence

Alignment Version 7.2.5 was used to verify the mutation. ClustalW Multiple Sequence was used to calculate and check the best matches of the mutation sequence to the wild-type of *hAR*. This way, wild-type *hAR* sequence and the mutation sequence can be seen, and the identities, differences and similarities can be identified. Mutant sequence that have the best similarity to the wild type are picked and are used to select the *DpnI*-digested DNA samples for BL21 (DE3) competent cells transformation.

2.3.8 Transformation of BL21 (DE3) competent *E.coli* cells

BL21 (DE3) *E.coli* cells are suitable for transformation and for protein expression. About 50μL of BL21 (DE3) bacterial glycerol stock was thawed and added to 2μL of *DpnI*-digested DNA in a 1.5mL microcentrifuge tube. The cell/DNA mixture was incubated on ice for 30 minutes, and was then heat shocked for 90 seconds at 42°C. Next the mutant mixture was placed on ice for 2 minutes; then 450μL of preheated SOC media was added to the mutant sample, and then incubated at 37°C for 60 minutes. Using a sterile spreader, 50μL of the sample reaction was plated on an LB-Ampicillin plate, and the plate was incubated overnight at 37°C.

2.3.9 Sodium-dodecyl-sulfate polyacrylamide gel electrophoresis (SDS-PAGE)

Following transformation of BL21 (DE3) competent *E.coli* cells, protein expression, purification and dialysis, the protein expression was checked by running the samples on a 10% SDS – PAGE gel. The gel was made up of 10mL of separating gel and

4mL of stacking gel. The composition of the separating and the stacking gel are shown below (Table 2.5 and Table 2.6).

Table 2.5: Separating Gel Reagent Compositions.

Reagents	Volume (mL)
Bisacrylamide/Acrylamide (30%)	3.4
Deionized water	3.8
Separating gel Buffer (1.5M Tris-HCl, pH 8.8)	2.6
10% SDS	0.1
Ammonium persulfate	0.1
TEMED	0.01

Table 2.6: Stacking Gel Reagent Compositions.

Reagents	Volume (mL)
Bisacrylamide/Acrylamide (30%)	0.67
Deionized water	2.7
Stacking gel Buffer (0.5M Tris-HCl, pH 6.8)	0.5
10% SDS	0.04
10% ammonium persulfate	0.04
TEMED	0.004

In running the gel of protein samples, the PageRuler Plus Prestained Protein Ladder served as the molecular weight marker, with a molecular weight range of 15kDa to 250kDa.

2.3.10 Protein Expression

Following the BL21 (DE3) cells transformation, a colony is picked from the LB-Ampicillin plate and inoculated into a 50mL 2XYT media containing 50μL of 100mg/mL Ampicillin. The mixture was then incubated by allowing it to shake overnight at 200 rpm and 37°C. After the overnight growth, about 10mL of the cell culture was inoculated into a 1L 2XYT media, and 1mL of 100mg/mL of Ampicillin is added, and incubated with

constant shaking in a rotary shaker at 240 rpm to reach an absorbance (A_{600}) of 0.6-0.8 at 37°C. About 1mL of the uninduced sample was saved from the media to be analyzed by SDS-PAGE. The protein expression was induced by supplementing 10mL of 100mM IPTG in the culture medium, and the culture was incubated for 4 hours at 200 rpm and 37°C. About 1mL of the induced protein sample was again saved to be analyzed by SDS-PAGE. The cells were harvested after 3-4 hours by centrifugation (6,000 rpm, 10 mins, 4°C) and the pellets were stored at -80°C. Each of the 1mL protein samples stored during the expression procedure were then spun in a microcentrifuge for about 2 minutes at 37°C, and then 60μL of 2x SDS protein sample buffer are added to the cell pellets individually. The mixture was boiled for 5 minutes to dissolve the pellets. About 3μL of the PageRuler Plus Prestained Protein Ladder was loaded on the first well of the gel, representing the molecular weight marker. About 25μL of each of the sample of the induced and the uninduced protein sample are then loaded on the preceding lanes and are then run in the vertical electrophoretic system. Staining and destaining of gel after electrophoresis are described following the protein purification section.

2.3.11 Sonication.

Harvested cells were thawed on ice and resuspended in extraction buffer (50mM Tris buffer (pH 7.0), containing 300mM NaCl and 2mM 2-mercaptoethanol. The slurry was vortexed to mix completely and the resultant suspension was placed in a beaker, which was then placed in another beaker containing ice. The set-up was placed in a sonicator to lyse the cells. The suspension was sonicated in two cycles: 30 seconds on to

lyse the cells, and allowed to cool for the next 30 seconds. This first cycle was repeated fifteen times. The second cycle involving a 60 seconds on and a 60 seconds off timing was repeated ten times to lyse the cell. The mutant *hAR* was isolated from the lysate separated by centrifugation at 12,000 rpm for 30 minutes at 4°C. The supernatant was collected in a bottle, and the process involving sonication and centrifugation was repeated twice to isolate all the protein from the cells. The resultant suspension was pooled together in one container.

2.3.12 Immobilized Metal Affinity Chromatography (TALON)

Following sonication, a 50mL gravity flow column was cleaned with 50mL of 2M NaOH, 50mL of ddH_2O, and 25mL of extraction buffer. The pooled supernatant from the sonication procedure containing hexa-His-*hAR* was mixed with 5mL of TALON CellThru metal affinity resin (IMAC). This resin, which was stored in 20% alcohol, was already washed with extraction buffer (20mL, three times) to wash out the alcohol, before mixing the resin with the supernatant. The mixture was incubated overnight by constant gentle shaking at 4°C. The affinity matrix slurry was passed through the cleaned column and the flow through was collected at a slow and a steady rate. Wash one, Wash two and Elution buffer already prepared were used for the elution. The column containing the protein was first washed with Wash one buffer containing 50mL of the components: 50mM Tris buffer (pH 7.0), 300mM NaCl and 2mM 2-Mercaptoethanol. About 50mL of the wash was collected. Another 50mL of the Wash two buffer containing 50mM Tris buffer (pH 7.0), 300mM NaCl, 2mM 2-Mercaptoethanol, and 10mM imidazole was again

used to wash the column. The protein was eluted with 300mM imidazole in 50mM Tris buffer (pH 7.0), containing 300mM NaCl and 2mM 2-Mercaptoethanol. The eluent was collected in a 10mL fraction from the column. The samples from this purification step were resolved on a 10% SDS gel. About 75µL of each sample was mixed with 25µL of the 4x SDS sample buffer, heated for 3 minutes in boiling water and loaded to the wells on a 10% SDS gel. The electrophoretic voltage was increased from 70 Volts to 100 Volts, as soon as the dye front crossed the separating gel. As soon as the dye front had run a sufficient distance from the negative electrode to the anode on the electrophoretic set up, the gel was removed and rinsed with water. The gel was then placed in a staining solution and microwaved for 45 seconds on high power, and allowed to shake in a shaker for 5 minutes. Destaining solution was then added and the gel was microwaved for another 45 seconds, and gently allowed to shake for 5 minutes. Three or more repetition of the destaining process was enough to visualize the gel on an ultraviolet illuminator.

2.3.13 Dialysis

Spectra/Por 1 dialysis tubing was boiled for about 5 minutes in deionized water. The purified protein was loaded into the dialysis bag and dialyzed for 8-12 hours in a 2L dialysis buffer (50mM Tris (pH 7.0), 300mM NaCl and 2mM 2-Mercaptoethanol) at 4°C. The dialysis buffer was changed three times and the protein was transferred into a 50mL falcon tube. The fraction after dialysis was again run on a 10% SDS gel, and viewed in an ultraviolet illuminator.

2.3.14 Protein Quantification by Bradford Reagent Assay.

Five dilutions of Quick Start Bovine Serum Albumin (BSA) protein standard, contained in a 2mL vials, were prepared. The solution was prepared in a 1.5mL microcentrifuge tubes, with a linear range of 0.2mg/mL to 1.0mg/mL in concentration. About 100μL of each of the standard and the sample protein solution where pipetted into a clean dry test tube, and 5mL of Quick Start Bradford 1x Dye Reagent were added to each tube and vortexed. The solution was incubated at room temperature for about 5 minutes and the absorbance of the solution was measured in triplicate at 595nm. The concentration of the protein was calculated from the standard curve obtained for the Bovine Serum Albumin (BSA), derived by plotting Abs_{595} versus protein concentration (mg/mL).

2.3.15 Thrombin Cleavage of Histidine Tag

Histidine Tag was removed by thrombin cleavage as per manufacturer's instruction. Following Bradford Assay for the determination of the protein concentration, 1μL of thrombin for every 4mg of protein was added to the purified protein, after dialysis, and the mixture was left to stand overnight at room temperature. About 5mL TALON metal affinity resin was mixed with the digested protein and allowed to shake at 4°C for about 16 hours to facilitate the binding of the resin to the protein. The matrix slurry was loaded on a gravity flow column, and a flow through was collected at a steady rate. The collected sample and a fraction of the dialyzed sample were ran on 10% SDS gel to verify the purity of the protein, representative of the appearance of thick bands in the lane in which the samples were loaded.

3.0 Enzyme Kinetics.

3.1 Aldehyde Reduction Kinetics of the Cys-298-Asn and the Cys-298-Glu Mutants.

3.2 Materials:

1mL Quartz Cuvette glassware (1.0 cm^2) was obtained from Sci Outlet, Tseunwan Hong Kong. DL-Glyceraldehyde, potassium phosphate (KH_2PO_4) and NADPH were obtained from Sigma Aldrich, 2-mercaptoethanol was obtained from Amresco Inc. Purified protein with histidine tag removed after thrombin cleavage. Deionized water and diode array spectrophotometer.

3.3 Buffers and Solutions.

The following stock solutions and buffers were prepared for the enzyme kinetics measurement: 50mL of 500mM KH_2PO_4 buffer (pH 6.2), 10mL of 100mM DL-Glyceraldehyde, 10mL of 7mM 2-mercaptoethanol, 15mL of 1.5mM NADPH and deionized water. The enzyme concentration was determined by Bradford assay for the Cys-298-Asn mutant enzyme and for the Cys-298-Glu mutant enzyme. The final working concentrations of the buffer and solutions were: 100mM potassium phosphate buffer (pH 6.2), 0.15 mM NADPH, and varied concentrations of DL-Glyceraldehyde.

3.4 Method:

To keep the purified protein at a reduced state, about 50μL of 7mM 2-mercaptoethanol was added to 500mL of the purified protein and then let to stand for about an hour. The aldehyde reduction activity of the Cys-298-Asn and Cys-298-Glu mutants at 25°C was monitored by UV spectrophotometry by measuring the decrease in the absorbance of the cofactor NADPH at 340nm. The spectrophotometer was set to a run time of 60 seconds, at 5 cycles, and was then blanked with a mixture of 600μL of deionized water, 200μL of DL-Glyceraldehyde, and 200μL of KH_2PO_4 buffer, all added to a 1mL quartz cuvette. To the 1mL cuvette, after blanking, varying enzyme volume (about 3-50μL), reduced with 2-mercaptoethanol, was pipetted. The 1mL mark was reached by adding the other components (DL-Glyceraldehyde, KH_2PO_4 buffer, and water). Using the Cys-298-Asn mutant enzyme, 450μL of water, 200μL of 100mM potassium phosphate buffer, 200μL of 100mM DL-Glyceraldehyde stock solutions were added into a 1mL cuvette, and 20μL of the reduced enzyme was also added to the mixture in the cuvette. The reaction was initiated by adding 130μL of NADPH was to the cuvette, and the change in absorbance at 340nm for 60 seconds was measured. This was done to determine the concentration and volume of the hAR mutant enzyme needed for an initial change in absorbance of 0.6-0.8. The absorbance was measured in duplicate. As this value was obtained, the volume of the enzyme (20μL) was kept constant, and the volume of the substrate (DL-Glyceraldehyde) was varied to monitor the decrease in absorbance with time. The varying substrate concentrations of DL-Glyceraldehyde used

were in the order: 0.05, 0.1, 0.50, 1.0, 5.0, 8.0, 12.0 and 20.0 mM for the Cys-298-Glu mutant enzyme, and 0.05, 0.1, 1.0, 5.0, 8.0. 10.0, 12.0 and 20.0 mM for the Cys-298-Asn mutant enzyme. For the 0.05mM concentration, 649.5 μL of deionized water, 0.5μL of 100mM DL-Glyceraldehyde, 20μL of hAR mutant enzyme (Cys-298-Asn), 200μL of 100mM potassium phosphate buffer and 130μL of NADPH were lastly added to the cuvette to initiate the reaction. The change in absorbance at 340nm for 60 seconds was then measured. Each individual measurement of these concentrations was evaluated in duplicate and the absorbance determined. The unit of enzyme activity was defined as μmol of NADPH oxidized/min. The changes in absorbance per minute were converted to μmol/min (rate). The aldehyde reduction reaction for the Cys-298-Asn and Cys-298-Glu mutant hAR was analyzed according to the Michaelis-Menten model for enzyme kinetics. The Michaelis-Menten constant K_m, the maximum velocity, V_{max}, for the substrate for the reduction reactions catalyzed by the mutant hAR enzyme were determined by plotting the rate of carbonyl reduction, v, versus substrate concentration, S, using the equation below.

$$v = \frac{V_{max} \cdot [S]}{(K_m + [S])}$$

The catalytic turnover number, k_{cat}, was evaluated from the ratio of $V_{max}/[E]$, where $[E]$ is the total enzyme concentration or the molar concentration of enzyme (from molecular weight and the weight/volume concentration). At least two determinations were performed for each kinetic constant. The rate of enzyme-dependent decrease in A_{340}nm was calculated using an extinction coefficient $e = 6220\ M^{-1}cm^{-1}$.

4.0 Results.

4.1 DNA Sequencing Results:

DNA sequencing results for the forward and the reverse sequence of the Cys-298-Asn mutant are shown below, on Figure 4.1 and Figure 4.2 respectively. Figure 4.3 and Figure 4.4 represents the DNA Sequencing results for the forward and the reverse sequence of the Cys-298-Glu mutant. The bases are represented in different colors and with precise protein coding sequence. The base A, shown in green, represents adenine, C, shown in blue represents cytidine, G shown in black represents guanine, and T shown in red represents thymidine. The dotted lines on the sequences represent undermined bases. The results show the DNA sequences of the mutants resolved by Eurofin genomics. The corresponding bases that each peak represents are then aligned with the bases of the wild-type and compared to check for correct mutation. Sequencing is important because it is the only way to determine the order of nucleotides within the mutant proteins that have been synthesized

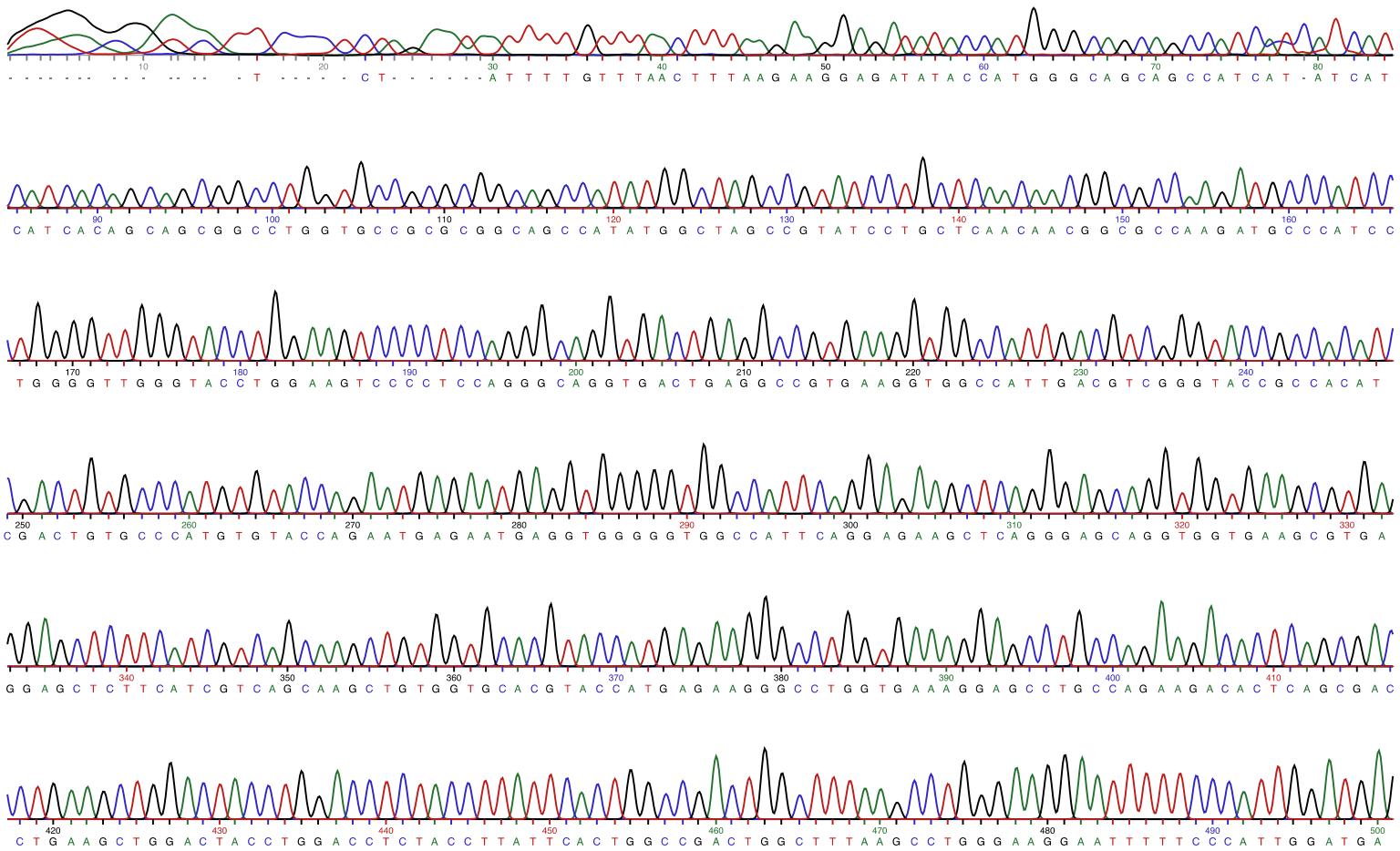

Figure 4.1 (Page 1) - DNA chromatogram for the forward sequence of Cys-298-Asn mutant.

Unpublished work: Ganesaratnam Balendiran, Sudipti Gupta, Emeka Udeigwe.

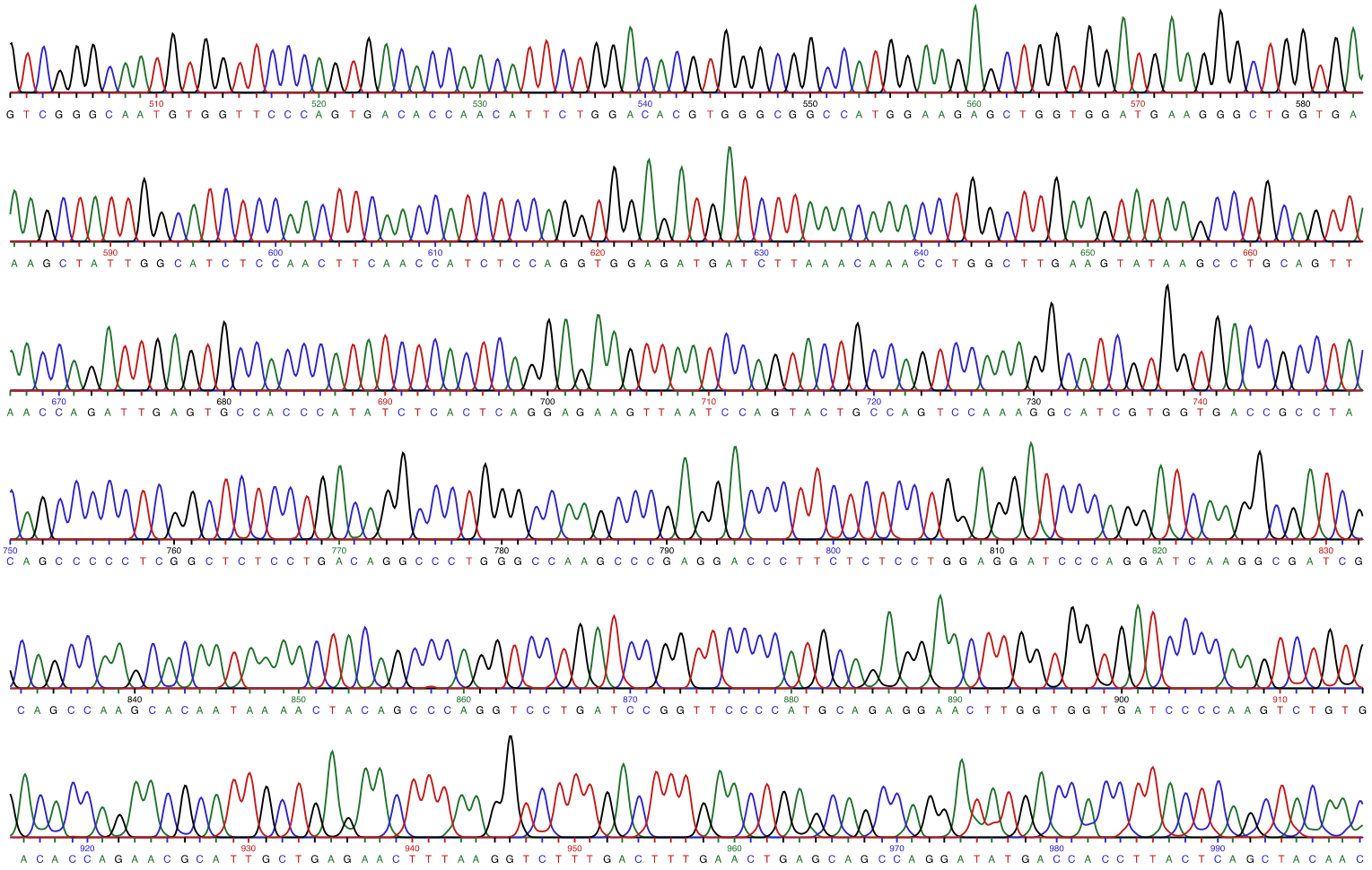

Figure 4.1 (Page 2) – DNA chromatogram for the forward sequence of Cys-298-Asn mutant.

Unpublished work: Ganesaratnam Balendiran, Sudipti Gupta, Emeka Udeigwe.

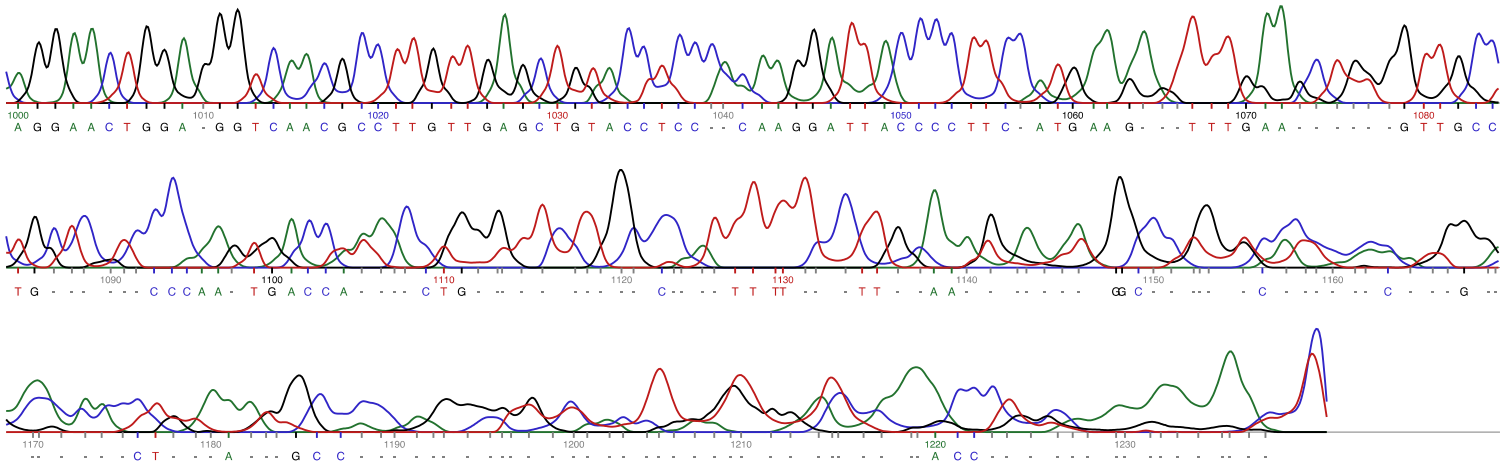

Figure 4.1 (Page 3) – DNA chromatogram for the forward sequence of Cys-298-Asn mutant

Unpublished work: Ganesaratnam Balendiran, Sudipti Gupta, Emeka Udeigwe

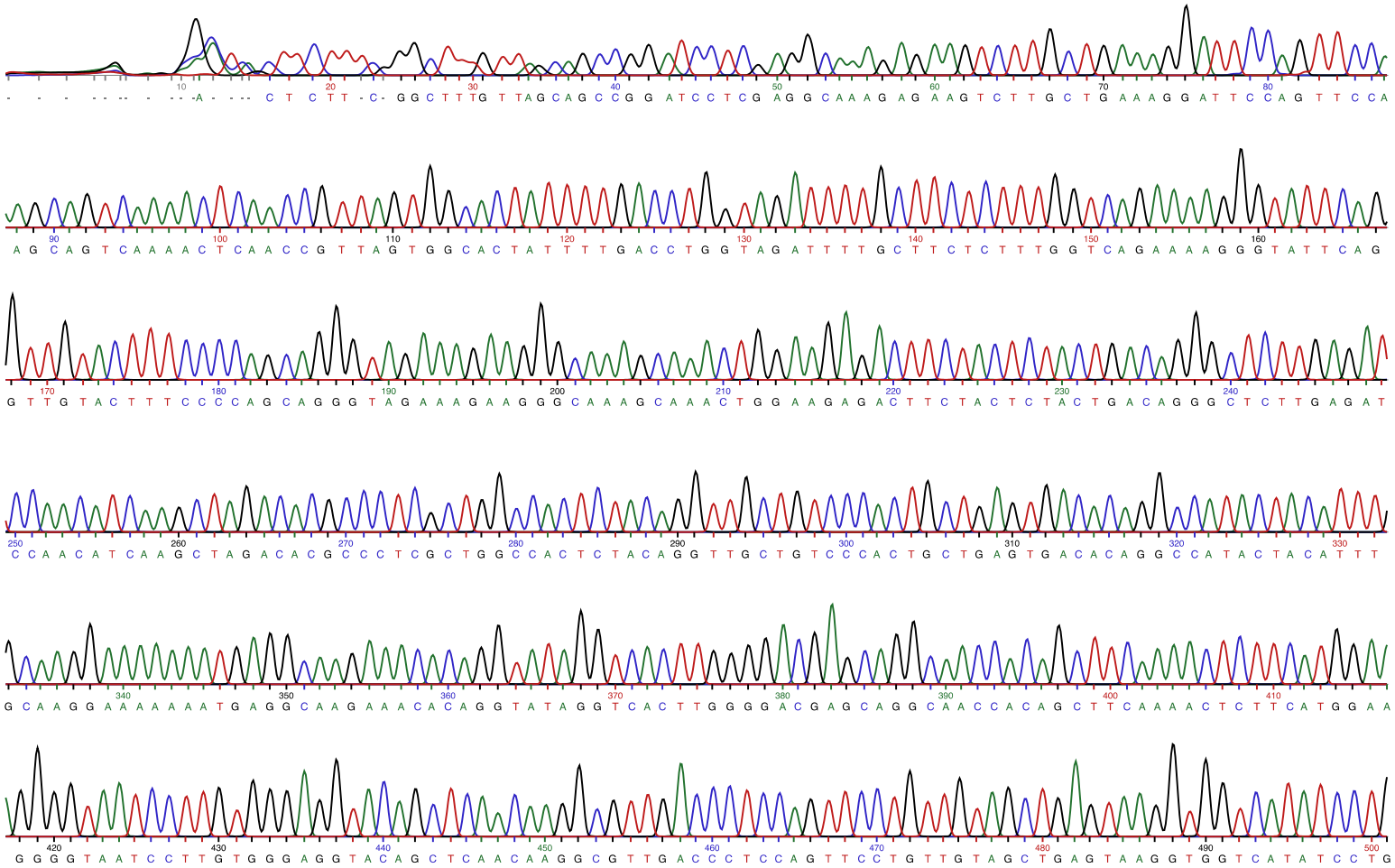

Figure 4.2 (Page 1) – DNA chromatogram for the reverse sequence of Cys-298-Asn mutant.

Unpublished work: Ganesaratnam Balendiran, Sudipti Gupta, Emeka Udeigwe.

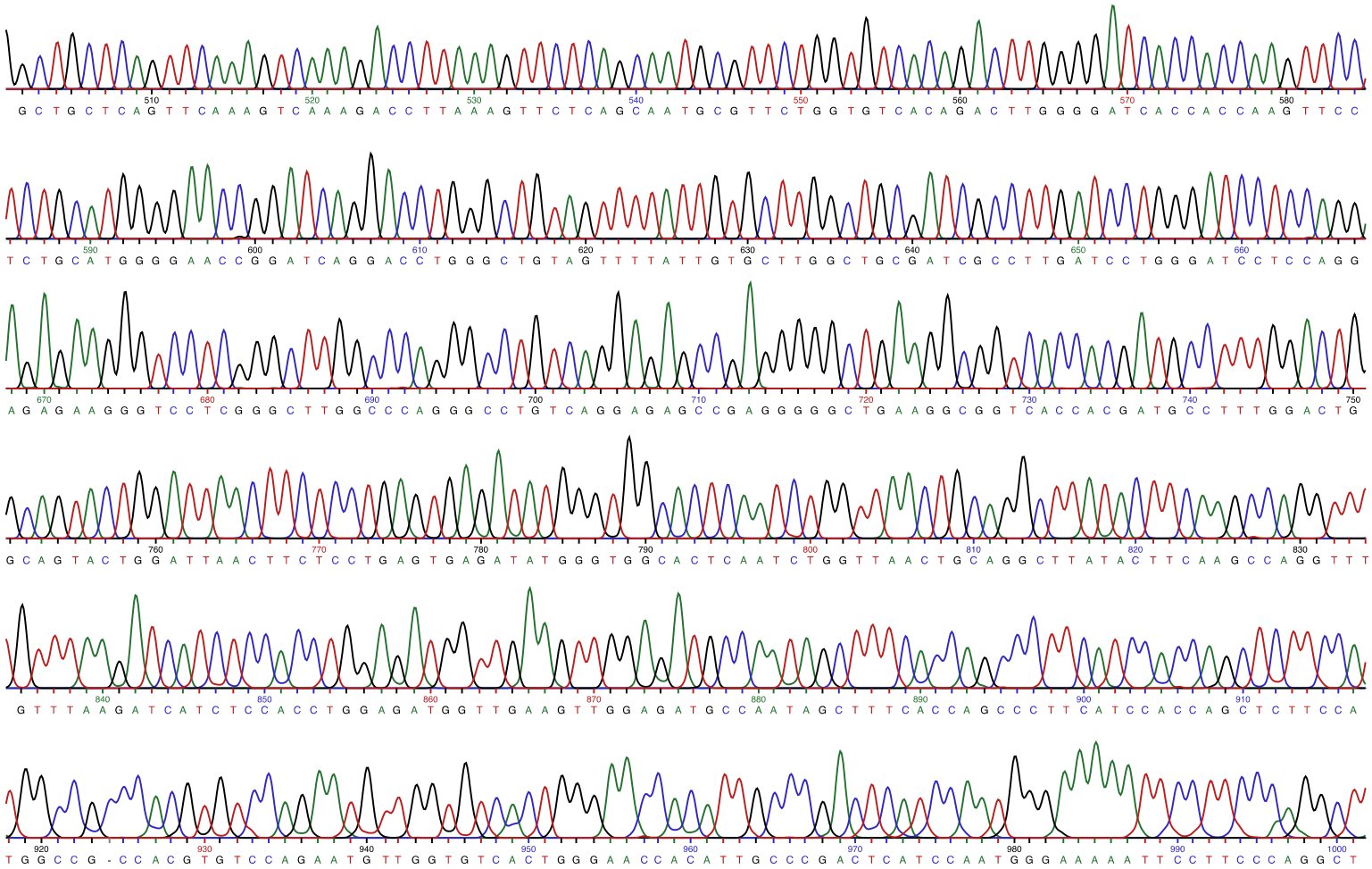

Figure 4.2 (Page 2) – DNA chromatogram for the reverse sequence of Cys-298-Asn mutant.

Unpublished work: Ganesaratnam Balendiran, Sudipti Gupta, Emeka Udeigwe.

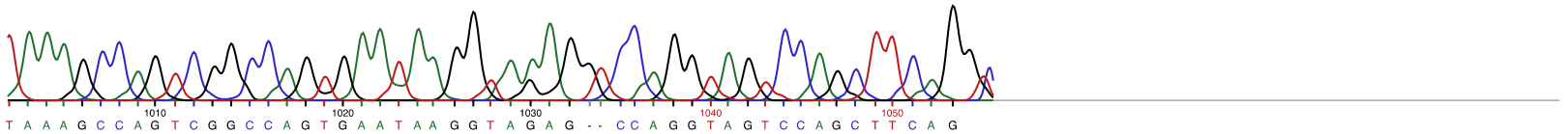

Figure 4.2 (Page 3) – DNA chromatogram for the reverse sequence of Cys-298-Asn mutant.

Unpublished work: Ganesaratnam Balendiran, Sudipti Gupta, Emeka Udeigwe.

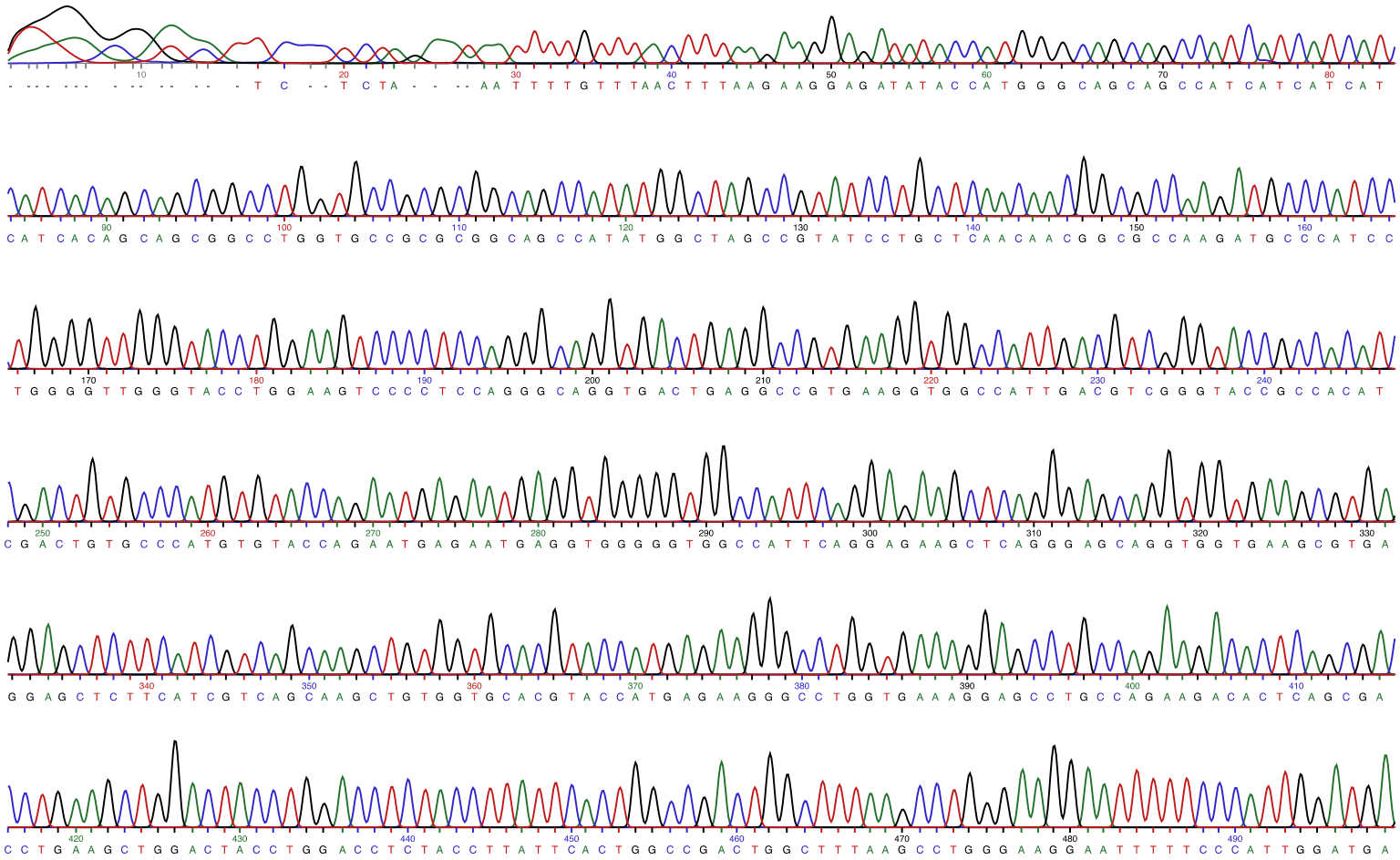

Figure 4.3 (Page 1) – DNA chromatogram for the forward sequence of Cys-298-Glu mutant.

Unpublished work: Ganesaratnam Balendiran, Sudipti Gupta, Emeka Udeigwe.

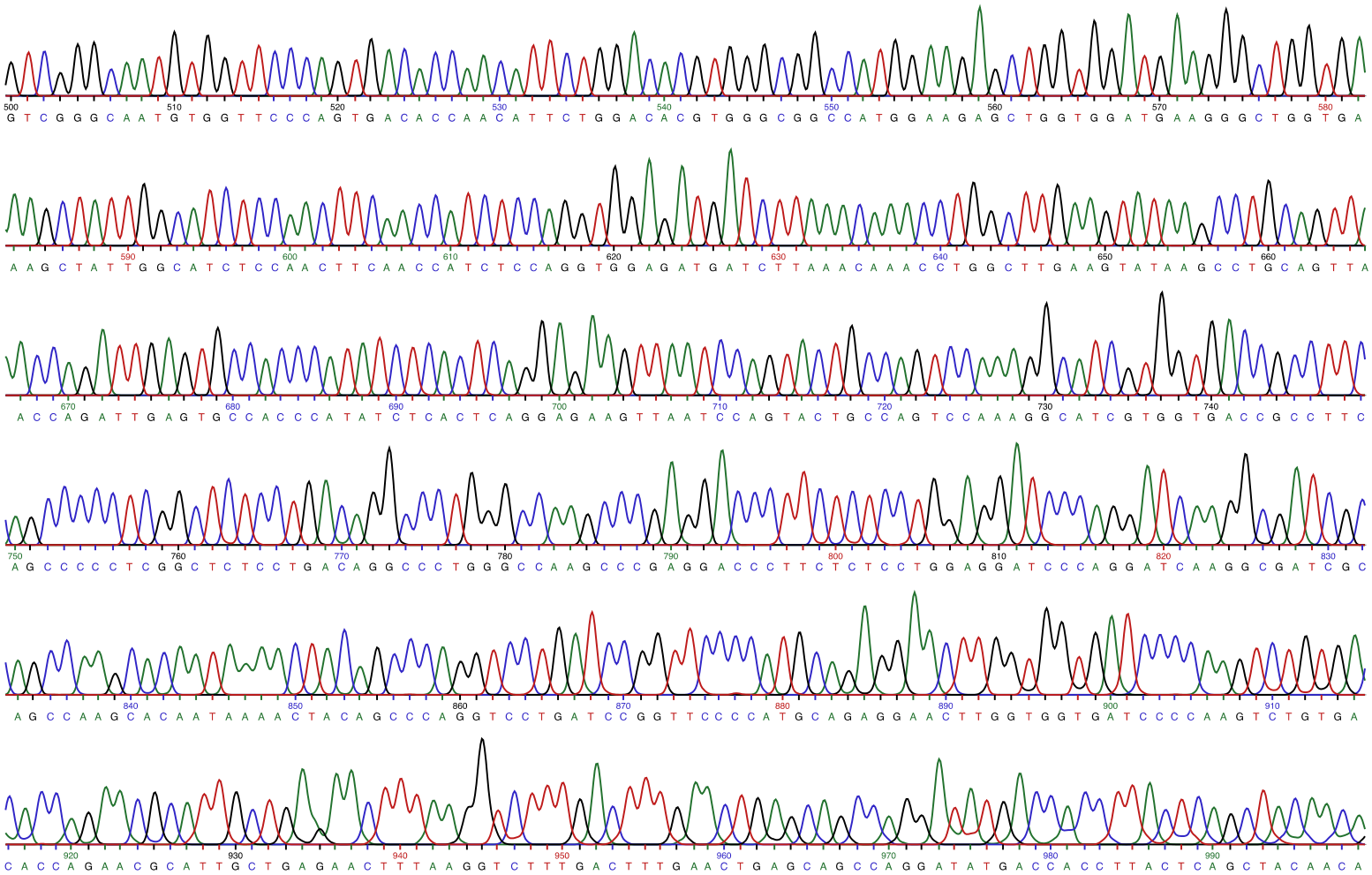

Figure 4.3 (Page 2) – DNA chromatogram for the forward sequence of Cys-298-Glu mutant.

Unpublished work: Ganesaratnam Balendiran, Sudipti Gupta, Emeka Udeigwe.

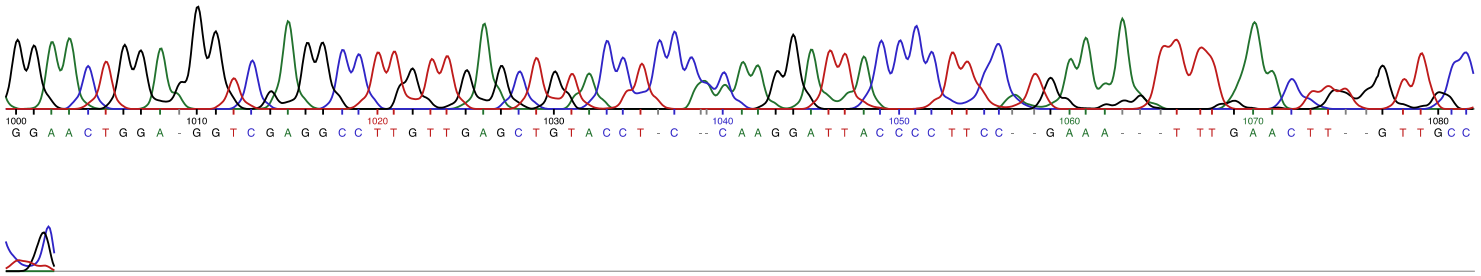

Figure 4.3 (Page 3) – DNA chromatogram for the forward sequence of Cys-298-Glu mutant.

Unpublished work: Ganesaratnam Balendiran, Sudipti Gupta, Emeka Udeigwe.

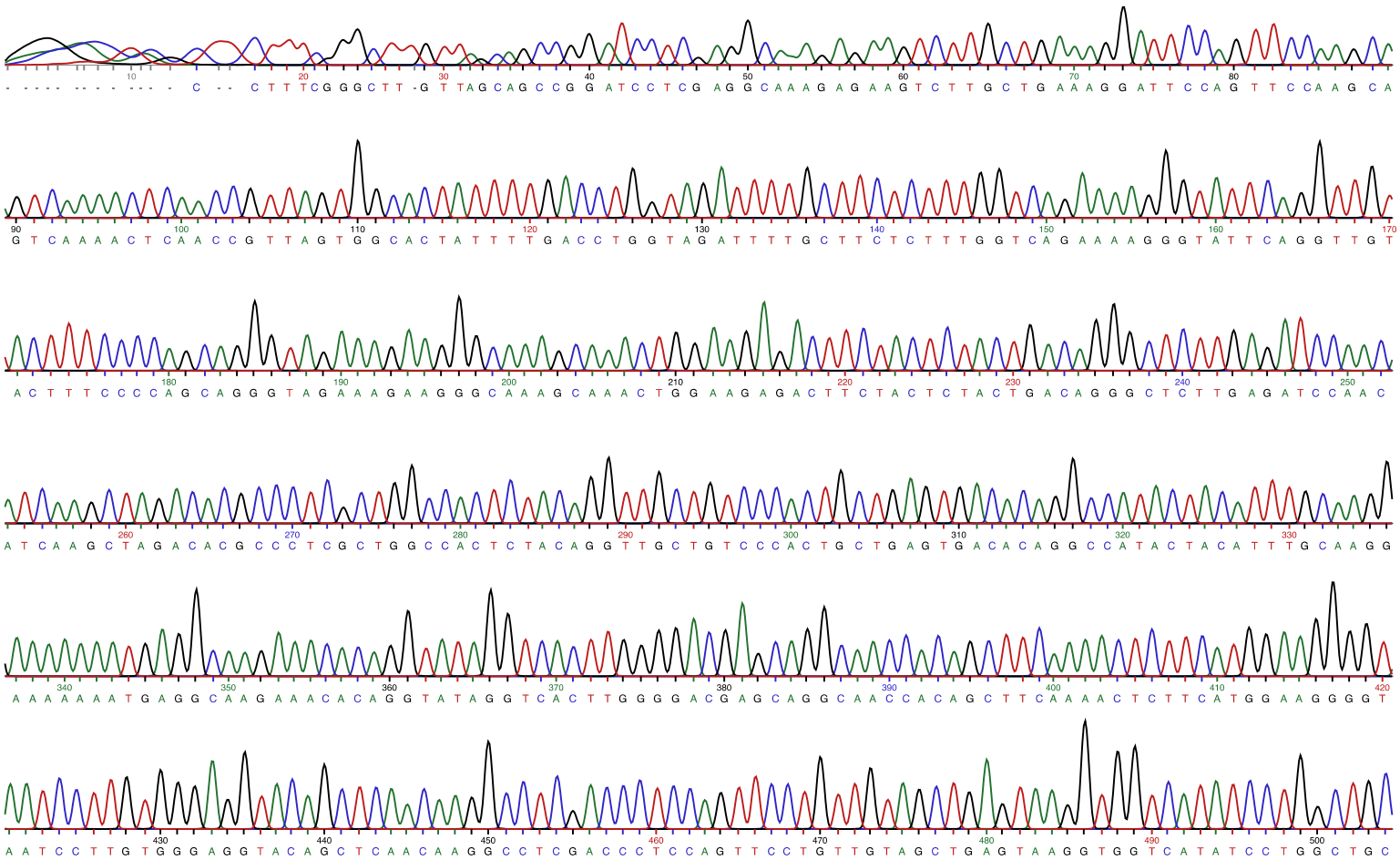

Figure 4.4 (Page 1) – DNA chromatogram for the reverse sequence of Cys-298-Glu mutant.

Unpublished work: Ganesaratnam Balendiran, Sudipti Gupta, Emeka Udeigwe.

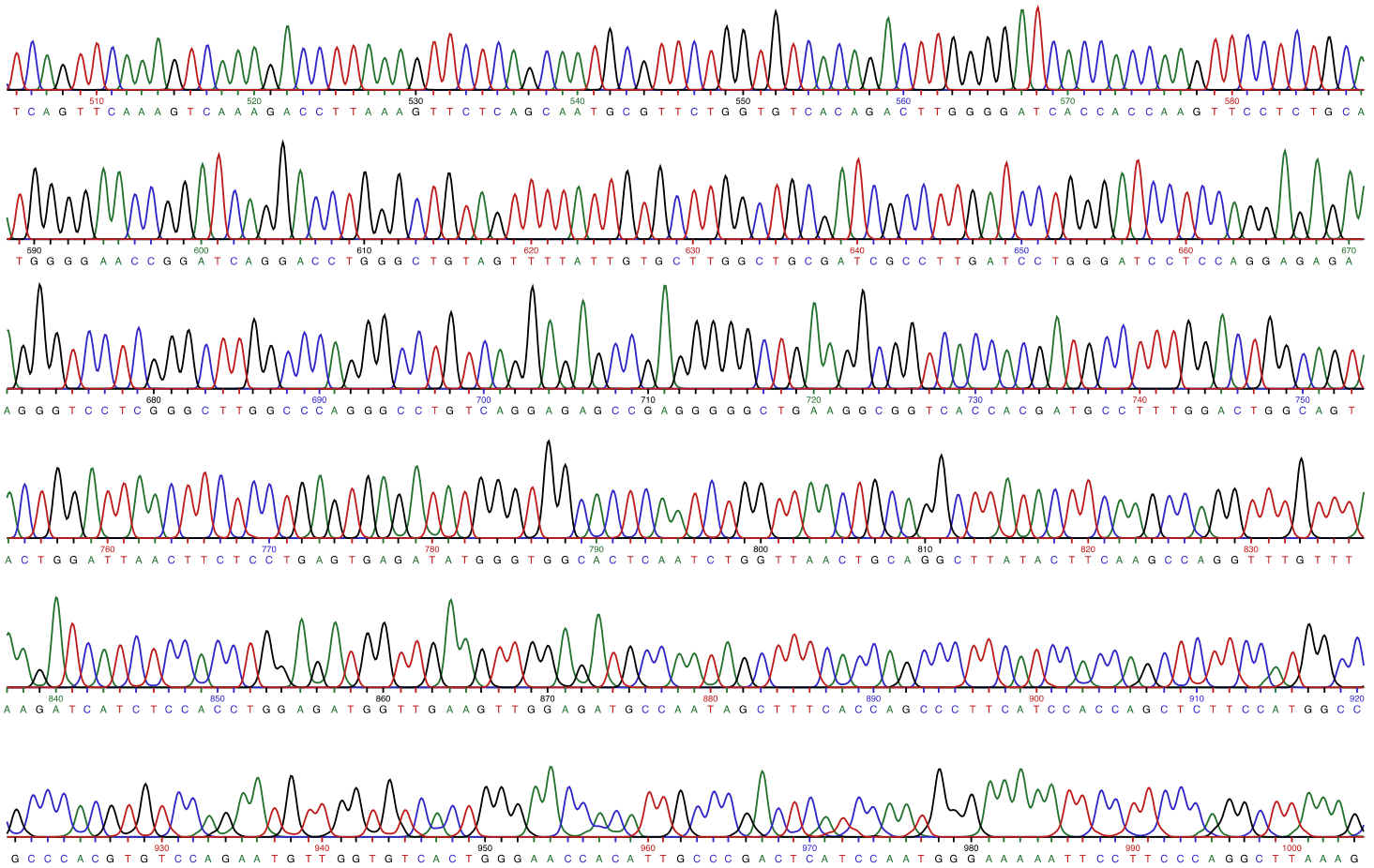

Figure 4.4 (Page 2) – DNA chromatogram for the reverse sequence of Cys-298-Glu mutant.

Unpublished work: Ganesaratnam Balendiran, Sudipti Gupta, Emeka Udeigwe.

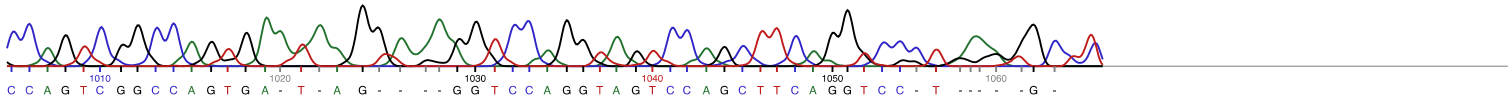

Figure 4.4 (Page 3) – DNA chromatogram for the reverse sequence of Cys-298-Glu mutant.

Unpublished work: Ganesaratnam Balendiran, Sudipti Gupta, Emeka Udeigwe.

4.2: Transformation of BL21 (DE3) competent *E.coli* cells:

Cys-298-Asn and Cys-298-Glu mutants hAR were expressed in *E. coli* BL21 cells that were grown in 2X-YT broth containing 100mg/mL of Amp (YT-Amp). After successful transformation by BL21 (DE3) competent *E.coli* cells, a colony was picked and streaked on an LB-Agar plate containing 100mg/mL of Ampicillin. Figure 4.5 and Figure 4.6 shows successful transformation after BL21 (DE3) cells were transformed. A single colony shown on the plate is picked and grown on a 2X YT media supplemented with 100mg/mL of ampicillin.

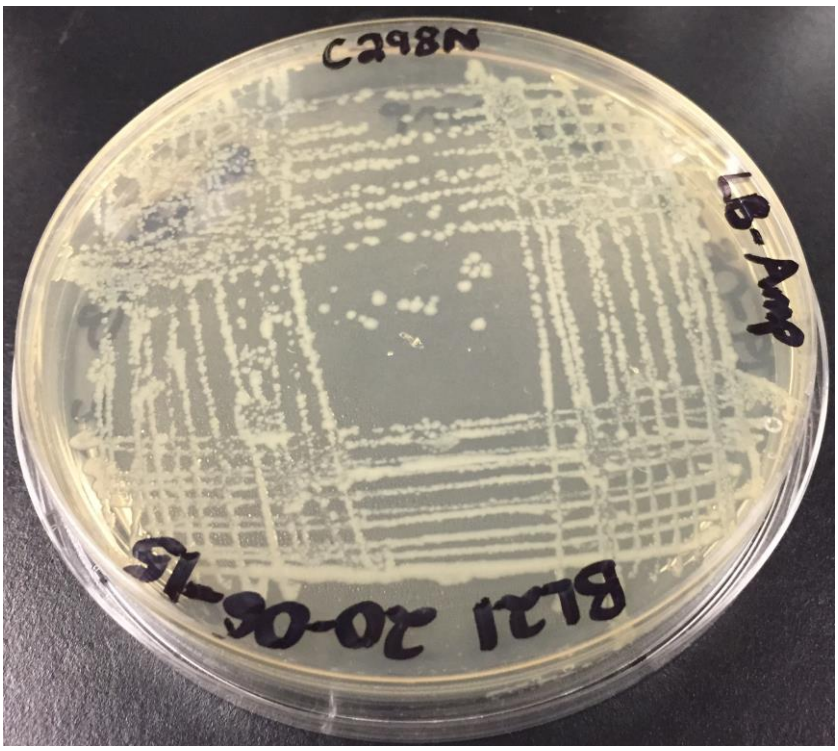

Figure 4.5: Luria Bertani - ampicillin plates containing colonies after successful BL21 (DE3) cells transformation for the Cys-298-Asn mutant enzyme.

Figure 4.6: Luria Bertani - ampicillin plates containing colonies after successful BL21 (DE3) cells transformation for the Cys-298-Glu mutant enzyme.

4.3 Protein expression:

Figure 4.7 contains uninduced samples of protein, and induced samples of protein after the supplementation of 1mM IPTG. Lane 1 contains the PageRuler Protein plus ladder, Lane 2 contains the uninduced sample, and Lane 3 and Lane 4 contains IPTG supplemeted (induced) sample.

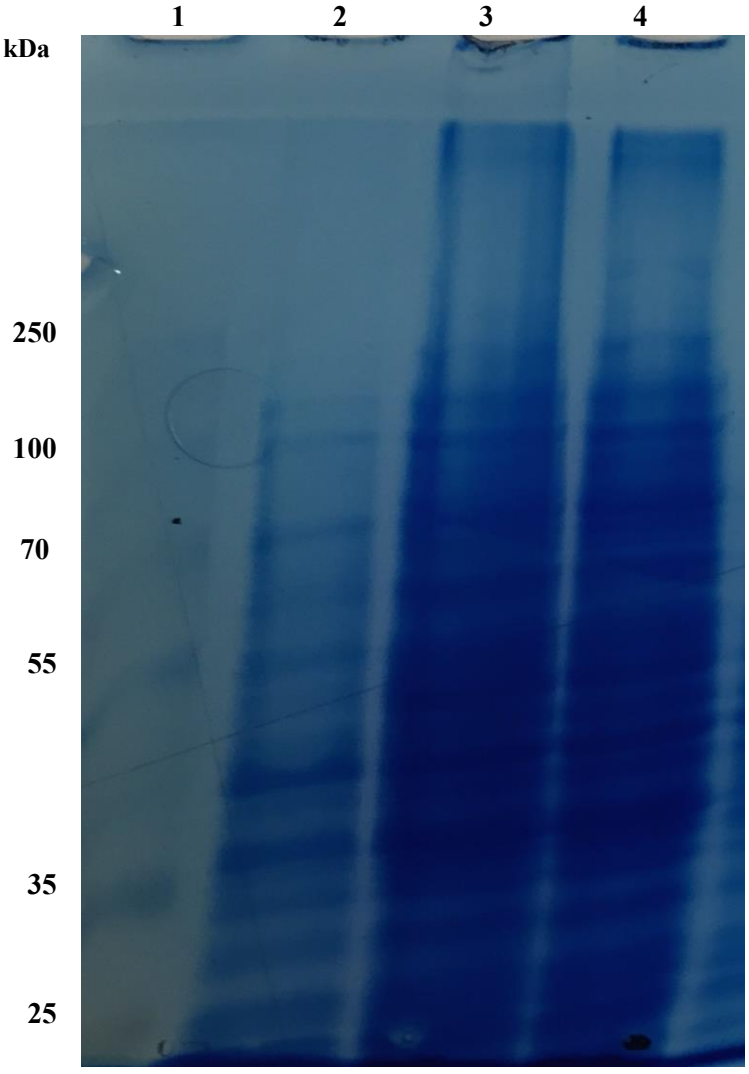

Figure 4.7: A gel picture of induced and uninduced sample collected after inducing protein expression with IPTG.

4.4 Immobilized Metal Affinity Chromatography:

The gel below (Figure 4.8) represents a typical 10% SDS-PAGE gel that was run after TALON Metal Affinity chromatography (IMAC) of the mutant enzyme, Cys-298-Asn. 10 wells are shown on the gel. Lane 1 represents the PageRuler Plus protein ladder. Lane 2 represents the flow-through collected subsequent to elution of the protein. Lane 3 represents the sample collected from the Wash one buffer. Lane 4 contains the sample obtained from the Wash two buffer. Lane 5, 6, 7, 8, and 9 contains samples obtained using elution buffer. The lane of interest is on Lane 5, with a thick protein band. The protein on this lane was collected and dialyzed against 2L of dialysis buffer containing 50mM Tris, pH 7.0, 300mM NaCl and 2mM 2-Mercaptoethanol, at 4°C. The thick band on lane 5 corresponds to a molecular weight of ~36kDa, correlating with the molecular weight of hAR. Lane 5 contains a thicker band because of the 50mL of elution buffer made, containing 300mM of imidazole; 10mL fraction of the protein was collected. The sample from Lane 5 was thicker than the sample on Lane 9, since it was collected first from the elution.

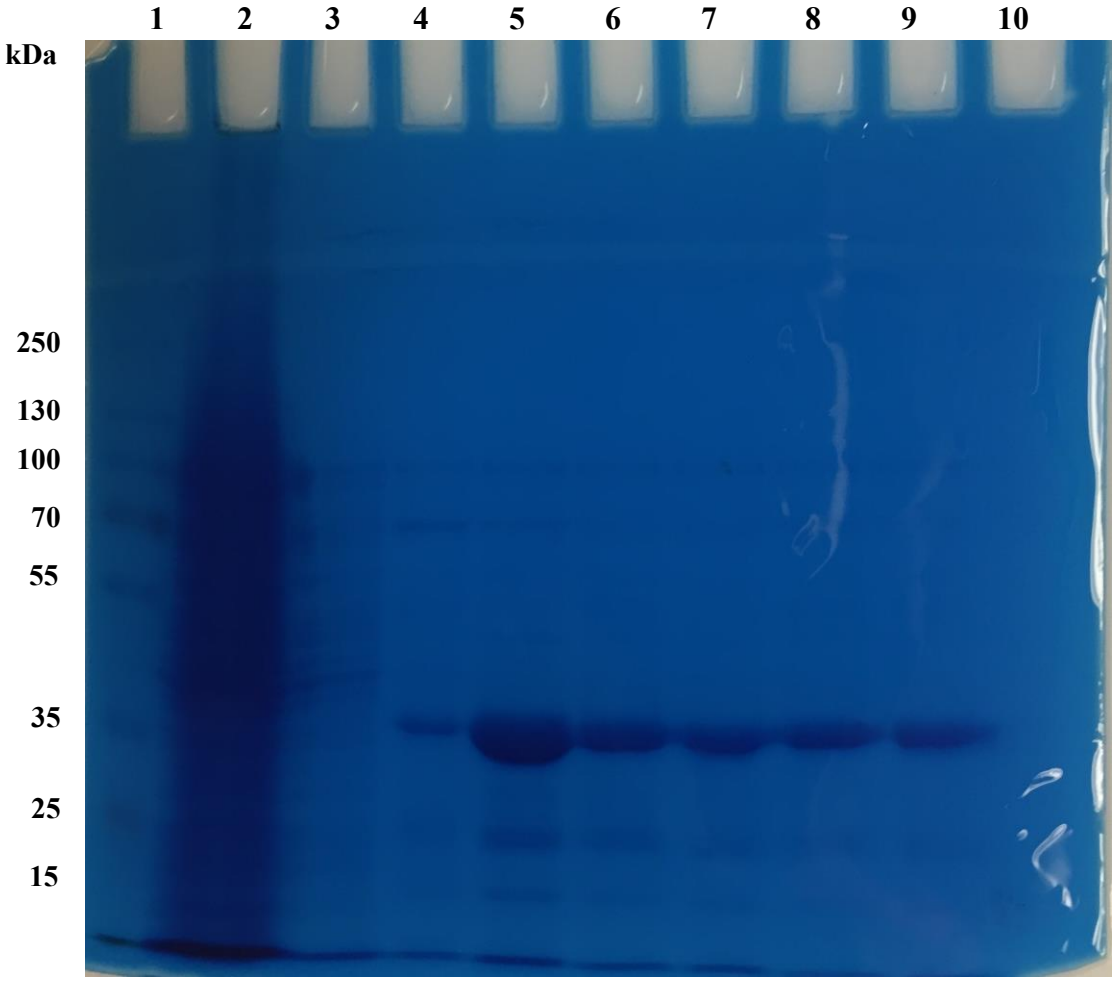

Figure 4.8: A gel picture of samples collected during purification of Cys-298-Asn mutant enzyme, using TALON metal affinity chromatography (IMAC) resin.

4.5 Protein Dialysis:

The collected fraction from IMAC purification as described above was dialyzed against a 2L dialysis buffer, with three buffer exchanges (for three days). Lane 1 represent the lane loaded with the PageRuler Protein plus standard (5-150 kDa). The thick band on Lane 2 corresponds to lane 5 from figure 4.8, after dialysis. The thick band corresponds to ~36kDa (35.858kDa).

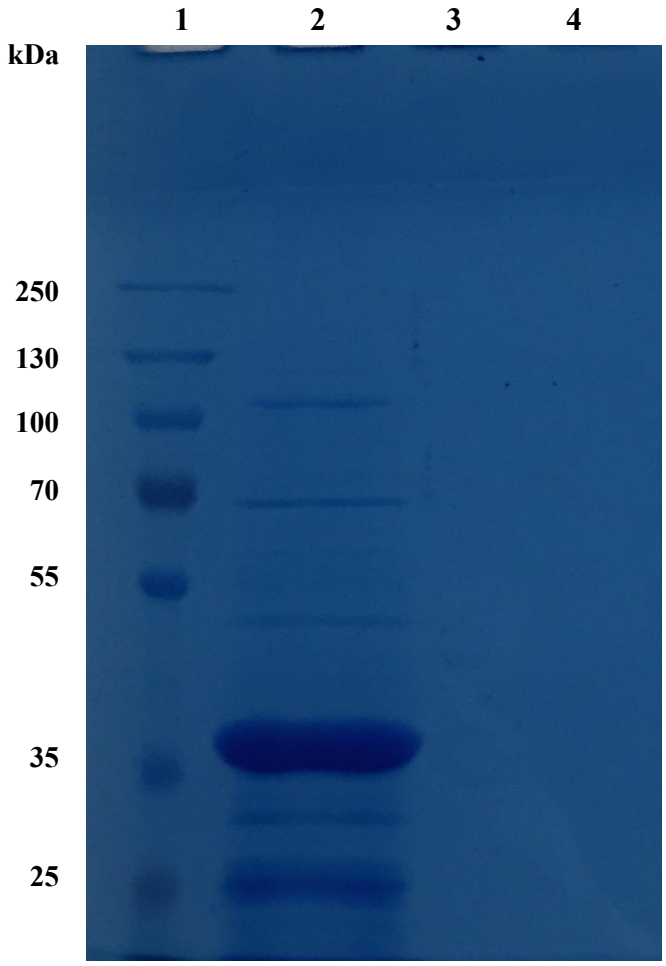

Figure 4.9: A gel picture of sample on lane 5 (Figure 4.8) obtained after dialysis of Cys-298-Asn mutant enzyme, using dialysis buffer.

4.6 Protein quantification: Bradford Reagent Assay:

Following purification of each mutant hAR enzyme, the concentration per volume of the protein was quantified using Bradford Assay. The Bio-Rad Protein Assay, based on the method of Bradford involves the addition of a Quick Start™ Bradford 1x Dye Reagent to the protein solution and the subsequent measurement of the mixture in a 1mL cuvette at 595nm, using a spectrophotometer. The standardized plot is then used to measure the concentration of the protein of interest.

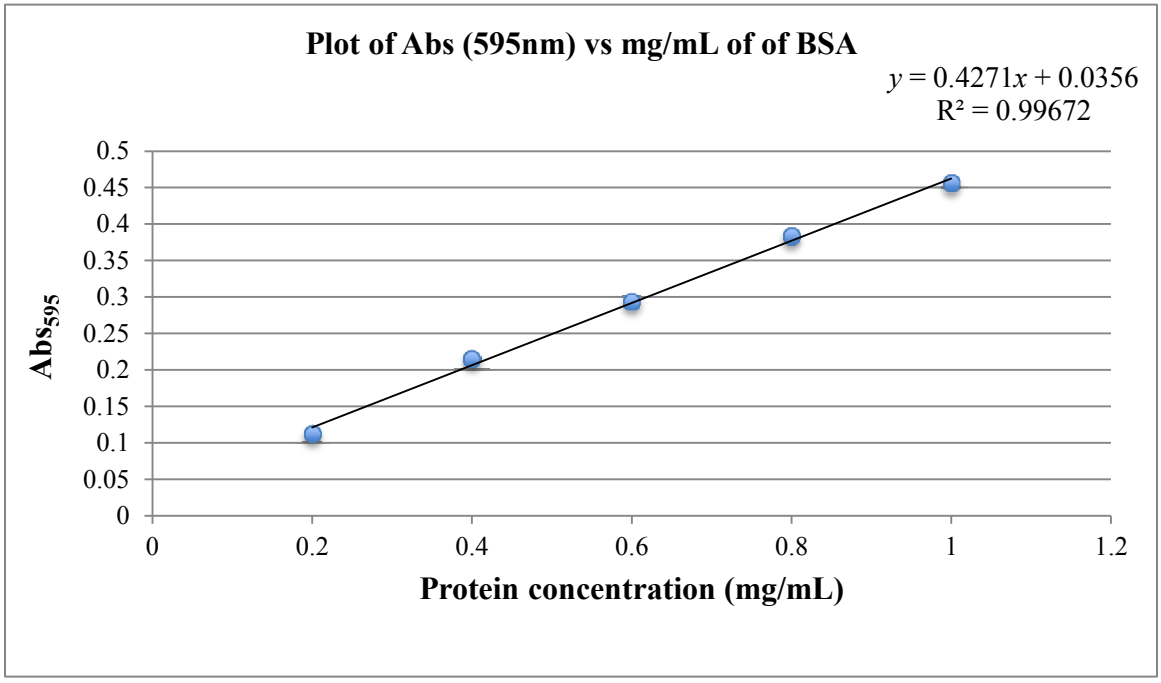

Figure 4.10: A typical BSA (Bovine Serum Albumin) standard curve for Bio-Rad protein concentration assay showing $Abs._{595}$ plotted against the concentration (mg/mL) of protein.

4.7 Thrombin Cleavage: 1μL of 10x thrombin cleavage enzyme was added to every 4mg of histidine-tag protein obtained after dialysis as described for thrombin cleavage in the method section. Lane 1 contains the PageRuler Plus Protein Ladder, while Lane 2 corresponds to the thrombin cleaved sample.

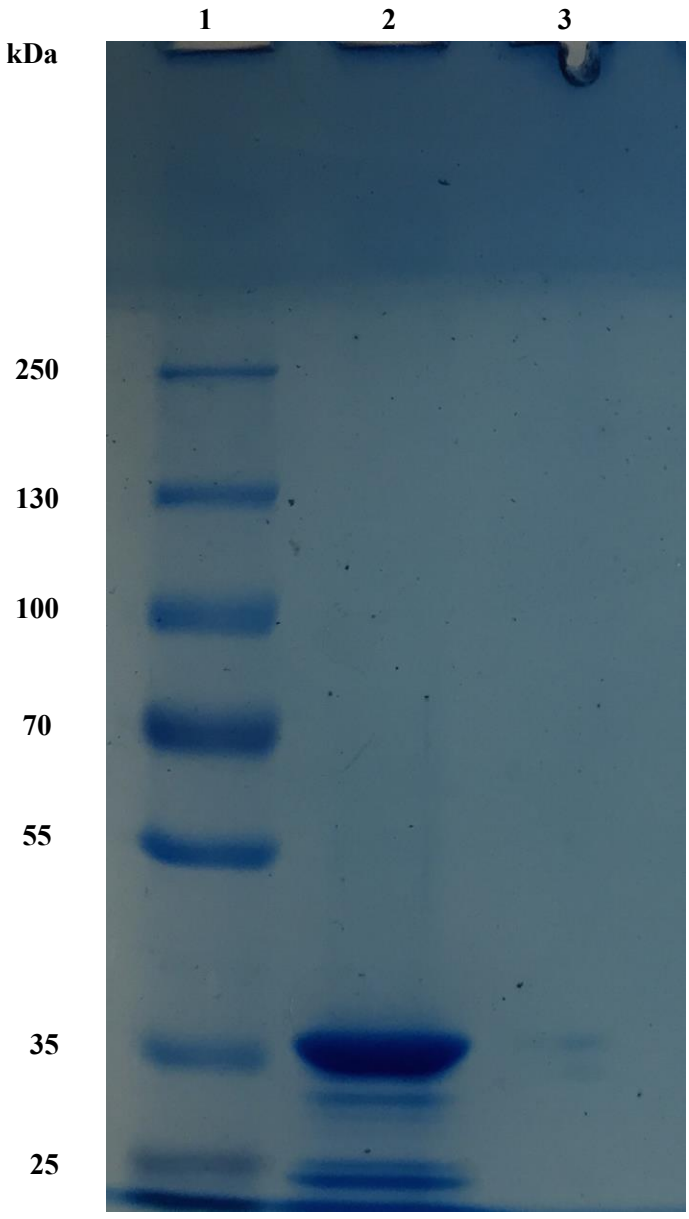

Figure 4.11: A 10% gel picture of a Cys-298-Asn thrombin cleaved protein sample.

4.8 Aldehyde reduction kinetics catalyzed by the Cys-298-Asn and the Cys-298-Glu mutant enzymes, using DL-Glyceraldehyde as substrate.

The results below show a typical result for the aldehyde reduction of the mutant hAR enzymes using DL-Glyceraldehyde as a substrate. The enzyme assay using the substrate was performed in duplicate. Values of K_m and k_{cat} were determined from the results of the initial increase in the rate of product formation using the equations,

$$v = \frac{V_{max} \cdot [S]}{(K_m + [S])}$$

The lineweaver-burk plot, or the double reciprocal plot, produced by taking the double reciprocal of both sides of the Michaelis-Menten equation was also plotted as $1/v$ against $1/[S]$. The plot is a linear form of the Michaelis-Menten equation, and produces a straight line equation, corresponding to the equation, $y = mx + c$. The y-intercept represents $1/V_{max}$, while the x-intercept represents $-1/K_m$.

Below is a representation of the Lineweaver-burk plot;

$$\frac{1}{v} = \frac{K_m}{V_{max}[S]} + \frac{1}{V_{max}}$$

The calculated k_{cat} and K_m are shown below. The comparison of the kinetic parameters for the wild-type (reported by Balendiran *et al*., 2011), and the Cys-298-Glu and Cys-298-Asn mutants indicate that the replacement of the cysteine in the wild-type with carboxylic group and carboxyamide group respectively, had considerable effects on the enzyme activities estimated using enzyme kinetics.

Table 4.1: Rates of reaction and average change in absorbance per unit time for the Cys-298-Asn mutants, with different substrate concentrations of DL-Glyceraldehyde.

[S] (mM)	$\Delta Abs_{340}/\Delta T$	*v* (nmol/min)	*v* (nmol/s)	1/*v*	1/[*S*]
0.05	0.0644	10.3554	0.1726	5.7941	20.0
0.10	0.1234	19.8344	0.3306	3.0250	10.0
1.00	0.3245	52.1850	0.8698	1.1498	1.00
5.00	0.3533	66.4559	1.1076	0.9029	0.20
8.00	0.4462	71.7333	1.1956	0.8364	0.13
10.0	0.4548	73.1139	1.2186	0.8206	0.10
12.0	0.4623	74.3196	1.2387	0.8073	0.08
20.0	0.4637	74.5599	1.2427	0.8047	0.05

Table 4.2: Rates of reaction and average change in absorbance per unit time for the Cys-298-Glu mutants, with different substrate concentrations of DL-Glyceraldehyde.

[S] (mM)	$\Delta Abs_{340}/\Delta T$	*v* (nmol/min)	*v* (nmol/s)	1/*v*	1/[S]
0.05	0.0421	6.7741	0.1129	8.8573	20.0
0.10	0.1245	20.0213	0.3337	2.9968	10.0
0.50	0.1753	28.1893	0.4698	2.1285	2.00
1.00	0.2012	32.3529	0.5392	1.8546	1.00
5.00	0.2901	46.6319	0.7772	1.2867	0.20
8.00	0.3307	53.1614	0.8860	1.1286	0.13
12.0	0.3752	60.3154	1.0053	0.9948	0.08
20.0	0.3791	60.9521	1.0159	0.9844	0.05

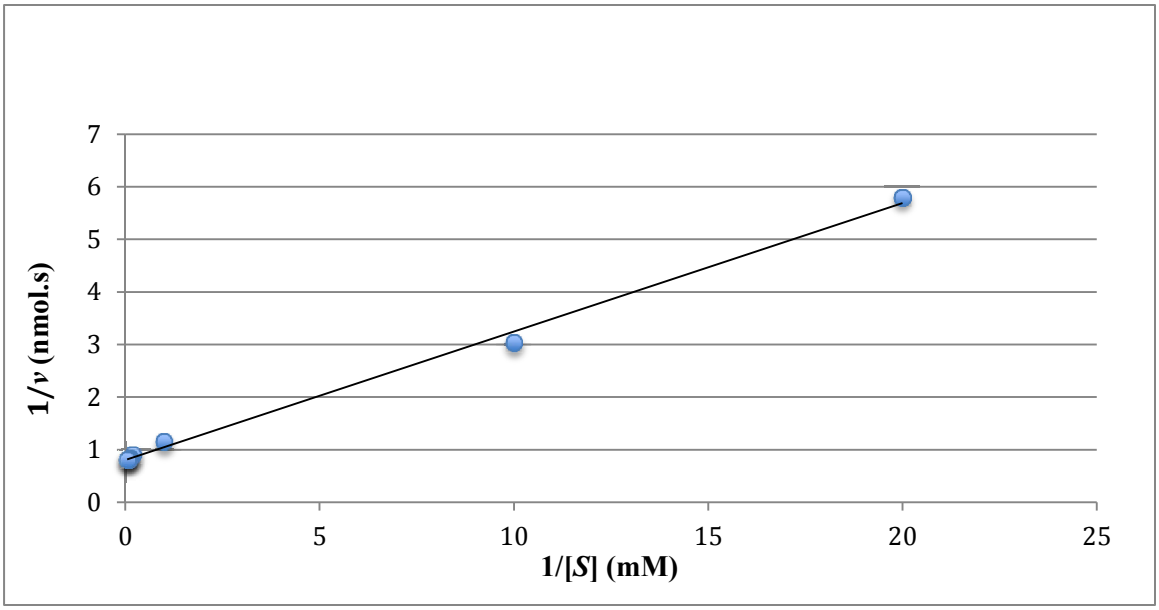

Figure 4.12: Lineweaver-burk plot of 1/*v* vs 1/[*S*] for the enzyme catalyzed reaction of the Cys-298-Asn mutant, using DL-Glyceraldehyde as substrate.

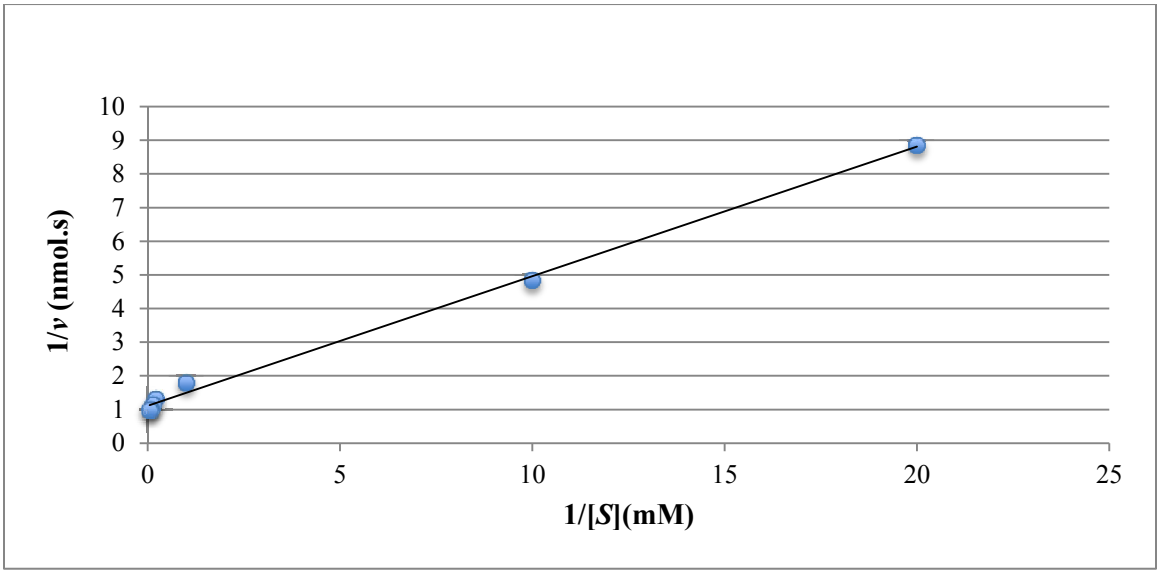

Figure 4.13: Lineweaver-burk plot of 1/*v* vs 1/[*S*] for the enzyme catalyzed reaction of the Cys-298-Glu mutant, using DL-Glyceraldehyde as substrate

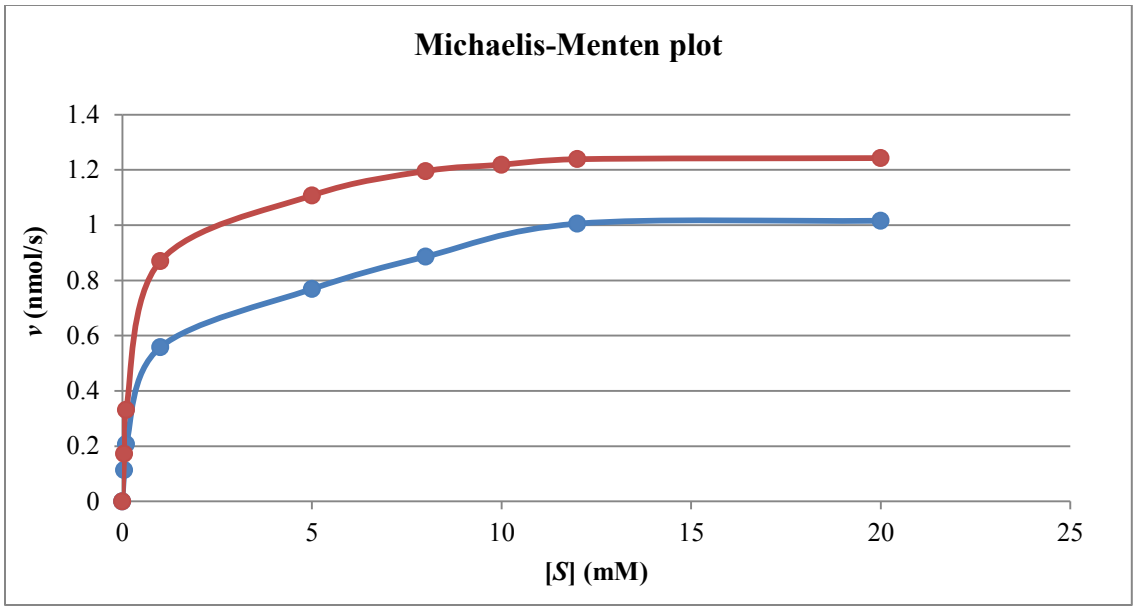

Figure 4.14: Michaelis-Menten kinetics for aldehyde reduction reaction catalyzed by the Cys-298-Glu (blue) and the Cys-298-Asn (red) hAR mutant enzyme, when DL-Glyceraldehyde was used as substrate.

Table 4.3: Kinetic parameters for the aldehyde reduction reaction catalyzed by the Cys-298-Asn and Cys-298-Glu mutant hAR enzymes in comparison to the enzyme activity of the wild-type.

Mutant	V_{max}(nmols^{-1})	k_{cat} (s^{-1})	K_m (mM)	k_{cat}/K_m(mM^{-1}s^{-1})
C298N	1.2076	4.4527	0.2525	17.6342
C298E	0.8943	0.7859	0.3440	2.2842
Wild-type [1]		1.55	0.1	14.5

5.0 Discussion

The Cys-298 mutants (Cys-298-Asn and Cys-298-Glu mutants) were successfully expressed in *E.coli* BL21 DE3 cells, and were later grown on a 2X YT media, containing 100mg/mL ampicillin, as the adequate media for the best expression of the enzyme. Successful transformants were selected on ampicillin plates.

BioEdit ClustalW multiple sequence alignment was efficiently used in aligning the sequences of the mutant with that of the wild-type in order to check for the correct mutation being effected. 10% SDS gel, used for SDS-PAGE was successful in determining the molecular weight corresponding to 36-kDa, as shown on the bands. Using immobilized metal affinity chromatography (TALON), which exhibits high affinity for histidine-tagged proteins, the protein of interest was purified as shown on the gels in the results section. The removal of histidine-tag in order to proceed with enzyme kinetics using thrombin, was successful, and is suggested by the reduction in the thickness of the band on a 10% SDS gel after thrombin digestion.

Bradford Reagent Assay, using Bovine Serum Albumin (BSA) was also adequate in assessing the concentration of the protein after purification and dialysis. The overall procedure utilized in mutant enzyme synthesis, overexpression and purification is highly improved and could be employed in future practices.

The kinetic contribution of the mutation of Cys-298-Asn and Cys-298-Glu is shown in Table 4.3. The K_m of the mutant enzyme Cys-298-Glu increased by approximately 3.4 – fold compared to the wild-type, while the K_m of the mutant enzyme Cys-298-Asn increased by approximately 60% compared to the wild-type. The increase in the K_m of the Cys-298-Glu mutant indicates the reduced affinity of the substrate DL-

Glyceraldehyde for the Cys-298-Glu mutant compared to the wild-type mutant. The Cys-298-Asn mutant is expected to minimally perturb the NADPH and substrate binding. Asparagine is a polar, hydrophilic, and neutral amino acid that is capable of participating in hydrogen bond with some residues on the active site of the enzyme; the increased K_m value of the Cys-298-Asn mutant using DL-Glyceraldehyde as substrate, although higher than the mutant form, Cys-298-Ser [1], reported by Balendiran *et al*., (2011) is similar in increase. Asparagine like serine is a polar non-charged amino acid residue, so this increase is expected. The possible reason for the increased K_m value for the Cys-298-Asn mutant compared to the wild-type may be due to the loose binding of NADPH to the Cys-298-Asn mutant enzyme, which is the first step in the catalysis of the enzyme, permitting less efficient re-orientation of the loops (residue 213-217) – rate limiting step of catalysis, and reduced formation of the binary complex in the forward reaction. Although the carboxyamide group of asparagine may be expected to form hydrogen bonds with some of the hydrophobic residues in the active site of the enzyme, where the mutant residue is located, the length of this bond is unknown to date. The k_{cat} increased about 65% for the Cys-298-Asn mutant when compared to the wild-type and the k_{cat}/K_m surprisingly increased by about 18% for the Cys-298-Asn mutant. The increased K_m (reduced $1/K_m$, and reduced affinity), increased k_{cat} and increased catalytic efficiency does not completely correlate with the kinetic parameters of the activated or oxidized hAR as has been reported earlier by other researchers, and does not match with that of the wild-type, for native hAR. The disparity in this correlation is only in terms of k_{cat}/K_m, which is mostly increasing for the oxidized enzyme form.

The turnover number, k_{cat}, decreased by about 49% for the Cys-298-Glu mutant compared to the wild-type. The catalytic efficiency k_{cat}/K_m, of the Cys-298-Glu mutant decreased by 85% for the Cys-298-Glu mutant enzyme compared to the wild-type. The corresponding increase in the K_m of the Cys-298-Glu mutant, by over 3-4 fold compared to the wild-type suggests the likelihood that the interaction of the NADPH with the enzyme is reduced, hence a subsequent reduction in the conformational change of the binding loop (residue 213-217) and less binding of substrate. These effects correlate with reduced binding affinity for the mutant using DL-Glyceraldehyde as substrate.

The carboxyl group of the glutamic acid mutant Cys-298-Glu, is expected to alter the active site environment, due to the steric hindrance provided by the large group. This disruption of the active site environment by this mutation could explain the increased K_m for DL-Glyceraldehyde as substrate. Reaction with certain inhibitors such as sorbinil, and a higher resolution of the structure of the Cys-298-Glu mutant as well as the structure of the Cys-298-Asn mutant and their interactions with the nicotinamide group, would provide a better understanding of the concomitant properties displayed by the mutants.

6.0 FUTURE WORK

Suggested future work could involve exploring the kinetic parameters of the Cys-298-Asn and the Cys-298-Glu mutants as described in the method section, using other substrates for the alcohol oxidation reaction such as benzyl alcohol, to understand any differences that might be displayed in the reverse reaction. Computational structures like omit maps could be used as well to elucidate the contribution of various mutations to the differences displayed in their kinetics. Furthermore, another area to focus on would be in inhibitor reactions using the mutants and some substrates. Currently, as one substrate has been explored, it may be pertinent to explore other substrates with different polar properties (hydrophobic or hydrophilic), in order to understand if the kinetic properties displayed are as a result of the polar similarities of the substrates to the enzymes.

7.0 REFERENCES

1. Balendiran, G. K., Michael, R. S., Frederick, P. S., Gomathinayagam, P., Richard, C., Malkhey, V., Duilio, C. The role of Cys-298 in aldose reductase function. *J. Biol. Chem.* **2011.** 286 (8), 6336-6344
2. Barnett, P. A., González, R. G., Chylack, L. T., Jr, Cheng, H-M. The Effect of Oxidation on Sorbitol Pathway Kinetics. *Diabetes*. **1986**, 35(4), 426–432.
3. Barski, O.A., Gabbay, K. H., Grimshaw, C. E., Bohren, K. M. Mechanism of Human Aldehyde Reductase: Characterization of the Active Site Pocket. *Biochemistry.* **1995,** 34(35), 11264-11275.
4. Bennett, M. J., Schlegel, B. P., Jez, J. M., Penning, T. M., Lewis, M. Structure of Alpha-Hydroxysteroid/Dihydrodiol Dehydrogenase Complexed with $NADP^+$. *Biochemistry*.**1996**, 35 (33), 10702–10711.
5. Bhatnagar, A., Liu, S. Q., Das, B., Srivastava, S. K. Involvement of Sulfhydryl Residues in Aldose Reductase-Inhibitor Interaction. *Mol. Pharmacol*. **1989,** 36 (6), 825–830.
6. Bhatnagar, A., Liu, S. Q., Ueno, N., Chakrabarti, B., Srivastava, S. K. Human Placental Aldose Reductase: Role of Cys-298 in Substrate and Inhibitor binding. *Biochim. Biophys. Acta.* **1994**, 1205 (2), 207–214.
7. Bhatnagar, S.-Q., Liu, J. M., Petrash, S. K., Srivastava, K. Mechanism of Inhibition of Aldose Reductase by Menadione. *Mol. Pharmacol*. **1992,** 42 (5), 917-921.
8. Bohren, K. M., Bullock, B., Wermuth, B., Gabbay, K. H. The Aldo-Keto

Reductase Superfamily, cDNAs and Deduced Amino Acid Sequences of Human Aldehyde and Aldose Reductases. *J. Biol. Chem*. **1989**, 264 (16), 9547–9551.

9. Bohren, K. M., Grimshaw, C. E., Lai, C. J., Harrison, D. H., Ringe, D, Petsko, G. A., Gabbay, K. H. Tyrosine-48 is the Proton Donor and Histidine-110 Directs Substrate Stereochemical Selectivity in the Reduction Reaction of Human Aldose Reductase: Enzyme Kinetics and Crystal Structure of the Y48H Mutant Enzyme. *Biochemistry*. **1994**, 33 (8), 2021–2032.
10. Bohren, K. M., Page, J. L., Shankar, R., Henry, S. P., Gabbay, K. H. Expression of Human Aldose and Aldehyde Reductases. Site-Directed Mutagenesis of a Critical Lysine-262. *J Biol Chem*.**1991**, 266 (35), 24031–24037
11. Borhani, D. W., Harter, T. M., Petrash J. M. The Crystal Structure of Aldose Reductase. NADPH Binary Complex. *J.Biol Chem*. **1992**, 267 (34), 24841-24847.
12. Bril, V., Buchanan, R. A. Long-term Effects of Ranirestat (AS-3201) on Peripheral Nerve Function in Patients with Diabetic Sensorimotor Polyneuropathy. *Diabetes Care.* **2006**, 29 (1), 68-72.
13. Brownlee, M. Biochemistry and Molecular Cell Biology of Diabetic Complications. *Nature.* **2001**, 414, 813–820.
14. Cappiello, M., Vilardo, P. G., Cecconi, I., Leverenz, V., Giblin, F. J., Del Corso, A., Mura, U., Occurrence of Glutathione-Modified Aldose Reductase in Oxidatively Stressed Bovine Lens. *Biochem. Biophys. Res. Commun*. **1995,** 207 (2), 775-782.

15. Cappiello, M., Voltarelli, M., Cecconi, I., Vilardo, P. G., Dal Monte, M., Marini, I., Del Corso, A., Wilson, D. K., Quiocho, F. A., Petrash, J. M., Mura, U. Specifically Targeted Modification of Human Aldose Reductase by Physiological Disulfides. *J. Biol. Chem.* **1996**, 271 (52), 33539-33544,
16. Cheng, H. M., González, R. G. The Effect of High Glucose and Oxidative Stress on Lens Metabolism, Aldose Reductase, and Senile Cataractogenesis. *Metab.Clin.Exp.* **1986,** 35 (4), 10–14.
17. Dixit, B. L., Balendiran, G. K., Watowich, S. J., Srivastava, S, Ramana, KV, Petrash, J. M., Bhatnagar, A., Srivastava, S. K., Kinetic and Structural Characterization of the Glutathione-Binding Site of Aldose Reductase. *J. Biol. Chem*. **2000**, 275 (28), 21587–21595.
18. Ehrig, T., Bohren, K. M., Prendergast, F. G., Gabbay, K. H. Mechanism of AldoseReductase Inhibition Binding of NADP+/NADPH and Alrestatin-Like Inhibitors. *Biochemistry*. **1994**, 33 (23), 7157–7165
19. Engerman, R. L., Kern T. S. Aldose Reductase Inhibition Fails to Prevent Retinopathy in Diabetic and Galactosemic Dogs. *Diabetes*. **1993**, 42 (6), 820–825.
20. Engerman, R. L., Kern, T. S. Experimental Galactosemia Produces Diabetic-like Retinopathy. *Diabetes*.**1984**, 33 (1), 97–100.
21. Felig, P. Disorders of Carbohydrate Metabolism. *Metabolic Control and Disease*. **1980**, 276–392.
22. Gabbay, K. H. Aldose Reductase Inhibition in the Treatment of Diabetic Neuropathy: Where are we in 2004? *Curr Diab. Rep.* **2004,** 4 (6), 405-408.

23. Gabbay, K. H. The Sorbitol Pathway and the Complications of Diabetes. *N. Engl. J. Med.* **1973**, 288(16), 831–836

24. Gabbay, K. H., Merola, L. O., Field, R. A. Sorbitol Pathway: Presence in Nerve and Cord with Substrate Accumulation in Diabetes. *Science*. **1966,** 151 (3707), 209–210.

25. Grimshaw, C. E. Aldose reductase: Model for a New Paradigm of Enzymic Perfection in Detoxification Catalysts. *Biochemistry*. **1992**, 31(42),10139-10145.

26. Grimshaw, C. E., Lai, C-J. Oxidized Aldose Reductase: In Vivo factor, not in Vitro Artifact. *Arch. Biochem. Biophys*. **1996,** 327 (1), 89-97.

27. Grimshaw, C.E., Bohren, K. M., Lai, C.-J., Gabbay, K. H. Human Aldose Rate Constants for a Mechanism Including Interconversion of Ternary Complexes by Recombinant Wild-Type Enzyme. *Biochemistry.* **1995a**. 34 (44), 14356-14365.

28. Grimshaw, C.E., Bohren, K. M., Lai, C.-J., Gabbay, K. H. Human Aldose Reductase: Subtle effects Revealed by Rapid Kinetic Studies of the C298A Mutant Enzyme. *Biochemistry.* **1995b,** 34 (44), 14366-14373

29. Harrison, D.H., Bohren, K.M., Ringe, D., Petsko, G.A., Gabbay, K. H. An Anion Binding Site in Human Aldose Reductase: Mechanistic Implications for the Binding of Citrate, Cacodylate, and Glucose 6-Phosphate. *Biochemistry.* **1994**, 33 (8), 2011-2020.

30. Heaseung, S. C., Sheng-Bing, W., Vidya, V., Christopher, I. M., Jennifer, E. V. E. Cysteine Oxidative Post-Transformational Modifications: Emerging Regulation in the Cardiovascular System. *Circ Res*. **2013**, 112 (2), 382-392.
31. Hers, H. G., Aldose Reductase. *Biochim. Biophys. Acta.* **1960**, 37, 120-126.
32. Hocker, B., Claren, J., Sterner, R., Mimicking Enzyme Evolution by Generating New (Betaalpha)8-Barrels from (betaalpha) 4-half-barrels. *Proc. Natl. Acad. Sci.* **2004**, 101 (47), 16448–16453.
33. Ishii, H., Tada, H., Isogai, S. An aldose reductase Inhibitor Prevents Glucose-Induced Increase in Transforming Growth Factor-Beta and Protein Kinase C Activity in Cultured Mesangial cells. *Diabetologia.* **1998**, 41 (3), 362–364.
34. Jez, J. M., Bennett, M. J., Schlegel, B. P., Lewis, M., Penning, T. M. Comparative Anatomy of the Aldo-Keto Reductase Superfamily. *Biochem. J.* **1997**, 326 (3), 625-636.
35. Kaiserova, K., Srivastava, S., Hoetker, J. D., Awe, S. O., Tang, X. L., Cai, J., Bhatnagar, A. Redox activation of aldose reductase in the ischemic heart. *J. Biol. Chem*. **2006**, 281 (22), 15110–15120.
36. Kaiserova, K., Tang, X. L., Srivastava, S., Bhatnagar, A. Role of Nitric Oxide in Regulating Aldose Reductase Activation in the Ischemic Heart. *J. Biol. Chem*. **2008**, 283 (14), 9101–9112.
37. Koya, D., King, G. L. Protein kinase C Activation and the Development of Diabetic Complications. *Diabetes.* **1998**, 47, 859–866.
38. Kubiseski, T. J., Hyndman, D. J., Morjana, N. A., Flynn, T. G. Studies on Pig Muscle Aldose Reductase. Kinetic mechanism and Evidence for a Slow

Conformational Change upon Coenzyme Binding. *J. Biol. Chem*. **1992**, 267(10), 6510–6517.

39. Liu, S. Q., Bhatnagar A, Srivastava SK. Carboxymethylation-Induced Activation of Bovine Lens Aldose Reductase. *Biochim. Biophys Acta*. **1992,** 1120 (3), 329–336.
40. Liu, S. Q., Bhatnagar, A., Srivastava, S. K. Does Sorbinil Bind to the Substrate Binding Site of Aldose Reductase? *Biochem. Pharmacol*. **1992**, 44 (12), 2427–2429.
41. Liu, S.Q., Bhatnagar, A., Srivastava, S. K. Bovine Lens Aldose Reductase: pH Dependence of Steady-State Kinetic Parameters and Nucleotide Binding. *J. Biol.Chem*. **1993**, 268 (34), 25494–25499.
42. Mara, L. The Polyol Pathway as a Mechanism for Diabetic Retinopathy: Attractive Elusive and Resilient. *Exp. Diabetes Res*. **2007**, 2007, 61038.
43. Nakano, T., Petrash J.M. Kinetic and spectroscopic evidence for active site inhibition of aldose reductase. *Biochemistry.* **1996,** 35 (34): 11196-111202.
44. Oates, P. J., Polyol Pathway and Diabetic Peripheral Neuropathy. *Int. Rev. Neurobiol*. **2002,** 50, 325–392.
45. Oleg, A. B., Srinivas, M. T., Aruni, B. The Aldo-Keto Reductase Superfamily and its Role in Drug Metabolism and Detoxification. *Drug Metabolism Reviews*. **2008**, 40 (4), 553-624.
46. Pawlowski, J. E., Penning, T. M. Overexpression and Mutagenesis of the Cdna for Rat-Liver 3-Alpha-Hydroxysteroid Dihydrodiol Dehydrogenase - Role of

Cysteine and Tyrosine in Catalysis. *J. Biol. Chem*. **1994**, 269 (19), 13502–13510

47. Petrash, J. M., Harter, T. M., Devine, C. S., Olins, P. O., Bhatnagar, A., Liu, S., Srivastava, S. K. Involvement of Cysteine Residues in Catalysis and Inhibition of Human Aldose Reductase. Site-Directed Mutagenesis of Cys-80, -298, and -303. *J. Biol.Chem.* **1992**, 267, 24833–24840.

48. Pollak, N., Dolle, C., Ziegler, M. The Power to Reduce: Pyridine Nucleotides – Small Molecules with a Multitude of Functions. *Biochem. J.* **2007**, 402 (2), 205-218.

49. Ramana, K. V, Chandra, D., Srivastava, S., Bhatnagar, A., Srivastava, S. K. Nitric oxide Regulates the Polyol Pathway of Glucose metabolism in Vascular Smooth Muscle Cells. *Faseb Journal*. **2003**, 17 (3), 417–425.

50. Ramana, K. V., Chandra, D., Srivastava, S., Bhatnagar, A., Aggarwal, B. B., Srivastava, S. K. Aldose Reductase Mediates Mitogenic Signaling in Vascular Smooth Muscle Cells. J. Biol. Chem. **2002**, 277 (35), 32063–32070

51. Ramana, K. V., Dixit, B. L., Srivastava, S. K., Balendiran, G. K., Bhatnagar, A. Selective Recognition of Glutathiolated Aldehyde Reductase. *Biochemistry*. **2000**, 39 (40), 12172-12180.

52. Ramana, K. V., Dixit, B. L., Srivastava, S., Bhatnagar, A., Balendiran, G. K., Watowich, S. J., Petrash, J. M., Srivastava, S. K. Characterization of the Glutathione Binding Site of Aldose Reductase. *Chem. Biol. Interact*. **2001**, 130–132 (1-3), 537–548.

53. Ramana, K. V., Tammali, R., Reddy, A. B., Bhatnagar, A., Srivastava, S. K. Aldose Reductase Necrosis Factor Alpha-Production is Essential for High Glucose-Induced Vascular Smooth Muscle Cell Growth. *Endocrinology*. **2007**,148 (9), 4371-4384.

54. Robison, W. G. Jr., Tillis, T. N., Laver, N., Kinoshita, J. H. Diabetes-Related Histopathologies of the Rat Retina Prevented with an Aldose Reductase Inhibitor. *Exp. Eye Res*. **1990**, 50 (4), 355–366.

55. Robison, W. G., Jr, Kador, P. F., Kinoshita, J. H. Retinal Capillaries: Basement Membrane Thickening by Galactosemia Prevented with Aldose Reductase Inhibitor. *Science*. **1983**, 21 (4616), 1177–1179.

56. Rondeau, J. M., Tête-Favier, F., Podjarny, A., Reymann, J. M., Barth, P., Beillmann, J. F., Moras, D. Novel NADPH-Binding Revealed by Crystal Structure of Aldose Reductase. *Nature.* **1992**, 355 (6359), 469-472.

57. Schlegel, B. P., Jez, J. M., Penning, T. M. Mutagenesis of 3 Alpha-Hydroxysteroid Dehydrogenase Reveals a "Push-Pull" Mechanism for Proton Transfer in Aldo-Keto Reductases. *Biochemistry*.**1998**, 37 (10), 3538–3548.

58. Schlegel, B. P., Ratnam, K., Penning, T. M. Retention of NADPH-Linked Quinone Reductase Activity in an Aldo-Keto Reductase Following Mutation of the Catalytic Tyrosine. *Biochemistry*.**1998**, 37 (31), 11003–11011.

59. Schrijvers, B. F., De Vriese, A. S., Flyvbjerg, A. From Hyperglycemia to Diabetic Kidney Disease: The Role of Metabolic, Hemodynamic, Intracellular Factors and Growth Factors/Cytokines. *Endocrv.Rev.* **2004,** 25 (6), 971–1010.

60. Srivastava S, Tammali R, Chandra D, Greer D. A., Ramana, K. V., Bhatnagar, A., Srivastava, S. K. Regulation of Lens Aldose Reductase Activity by Nitric Oxide. *Exp.Eye Res*. **2005**, 81 (6), 664–672.

61. Srivastava, S. K., Ansari, N. H., Bhatnagar, A., Hair, G., Liu, S.-Q., Das, B. Activation of Aldose Reductase by Non-Enzymatic Glycosylation. *Prog. Clin. Biol. Res.* **1989**, 304, 171-184.

62. Srivastava, S., Chandra A, Bhatnagar A, Srivastava SK, Ansari NH. Lipid Peroxidation Product, 4-hydroxynonenal and its Conjugate with GSH are Excellent Substrates of Bovine Lens Aldose Reductase. *Biochem Biophys Res Commun.* **1995**, 217 (3), 741–746.

63. Srivastava, S., Chandra, A., Ansari, N. H., Srivastava, S. K., and Bhatnagar, A. Identification of cardiac oxidoreductase(s) involved in the metabolism of the lipid peroxidation-derived aldehyde-4-hydroxynonenal. *Biochem. J.* **1998** 329 (3), 469–475.

64. Srivastava, S., Dixit, B. L., Ramana, K. V., Chandra, A., Chandra, D., Zacarias, A., Petrash, J. M., Bhatnagar, A., Srivastava, S. K. Structural and Kinetic Modifications of Aldose Reductase by S-nitrosothiols. *Biochem. J*. **2001**, 358 (1), 111–118.

65. Szwergold, B. S., Kappler, F., Brown, T. R. Identification of Fructose 3-Phosphate the Lens of Diabetic Rats. *Science*. **1990**, 247(4941), 451–454

66. Vander Jagt, D. L., Hunsaker, L. A., Robinson, B., Stangebye, L. A., Deck, L. M. Aldehyde and Aldose Reductases from Human Placenta: Heterogeneous

Expression of Multiple Enzyme Forms. *J Biol Chem*. **1990**, 265(19), 10912–10918.

67. Vander Jagt, D. L., Robinson, B., Taylor, K. K., Hunsaker, L. A. Reduction of Trioses by NADPH-Dependent Aldo-keto Reductases. Aldose Reductase, Methylglyoxal, and Diabetic Complications. *J. Biol Chem*.**1992**, 267 (7), 4364–4369
68. Vega, M. C., Lorentzen, E., Linden, A., Wilmanns, M. Evolutionary Markers in the (Beta/Alpha)8-Barrel Fold. *Curr. Opin. Chem. Biol*. **2003**, 7 (6), 694–701.
69. Wendt, T., Bucciarelli, L., Qu, W., Lu, Y., Yan, S. F., Stern, D. M., Schmidt, A. M. Receptor for Advanced Glycation Endproducts (RAGE) and Vascular Inflammation: Insights into the Pathogenesis of Macrovascular Complications in Diabetes. *Curr. Atheroscler. Rep.* **2002**, 4 (3), 228–237.
70. Wermuth, B., Monder, C. Aldose and Aldehyde Reductase Exhibit Isocorticosteroid Reductase Activity. *Eur J Biochem*. **1983**, 131 (2), 423–426.
71. Williamson, J. R., Chang, K., Frangos, M., Hasan, K. S., Ido, Y., Kawamura, T., Nyengaard, J. R., Van den E. M., Kilo, C., Tilton, R. G. Hyperglycemic Pseudohypoxia and Diabetic Complications. *Diabetes*. **1993,** 42(6), 801–813.
72. Wilson D. K., Tarle, I., Petrash, J. M., Quiocho, F.A.Refined 1.8 A Structure of Human Aldose Reductase Complexed with the Potent Inhibitor Zopolrestat. **1993**. 90 (21), 9847-9851.
73. Wilson, D. K., Bohren, K. M., Gabbay, K. H., Quiocho, F. A. An Unlikely Sugar Substrate Site in the 1.65Å Structure of the Human Aldose Reductase

Holoenzyme Implicated in Diabetic Complications. *Science*. **1992**, 257 (5066), 81–84.

74. Ye, Q., Hyndman, D., Green, N.C, Li, L., Jia, Z., Flynn, T.G. The crystal structure of an aldehyde reductase Y50F mutant-NADP complex and its implications for substrate binding. *Chem Biol Interact*. **2001**,130–132(1–3), 651–658